LBL-15984
Preprint c.2

Lawrence Berkeley Laboratory

UNIVERSITY OF CALIFORNIA

RECEIVED
LAWRENCE
BERKELEY LABORATORY

JUL 5 1983

LIBRARY AND
DOCUMENTS SECTION

Materials & Molecular Research Division

To be published as a chapter in a CHEMICAL REACTION ENGINEERING Handbook, edited by A. Varma and T. Carberry, Notre Dame University

ELECTROCHEMICAL REACTION ENGINEERING

G.G. Trost, V. Edwards, and J. Newman

May 1983

TWO-WEEK LOAN COPY

This is a Library Circulating Copy which may be borrowed for two weeks. For a personal retention copy, call Tech. Info. Division, Ext. 6782.

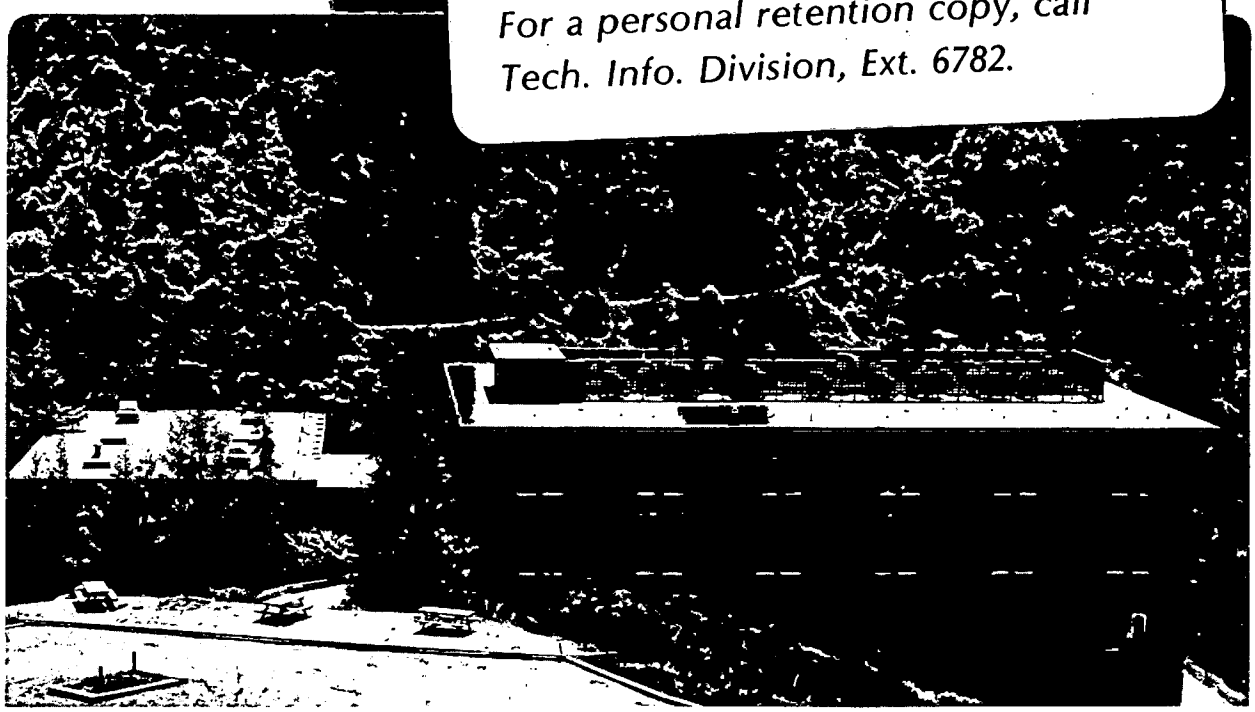

Prepared for the U.S. Department of Energy under Contract DE-AC03-76SF00098

LBL-15984 c.2

DISCLAIMER

This document was prepared as an account of work sponsored by the United States Government. While this document is believed to contain correct information, neither the United States Government nor any agency thereof, nor the Regents of the University of California, nor any of their employees, makes any warranty, express or implied, or assumes any legal responsibility for the accuracy, completeness, or usefulness of any information, apparatus, product, or process disclosed, or represents that its use would not infringe privately owned rights. Reference herein to any specific commercial product, process, or service by its trade name, trademark, manufacturer, or otherwise, does not necessarily constitute or imply its endorsement, recommendation, or favoring by the United States Government or any agency thereof, or the Regents of the University of California. The views and opinions of authors expressed herein do not necessarily state or reflect those of the United States Government or any agency thereof or the Regents of the University of California.

LBL-15984

Electrochemical Reaction Engineering

Gary G. Trost, Victoria Edwards, and John Newman

Materials and Molecular Research Division
Lawrence Berkeley Laboratory, and
Department of Chemical Engineering
University of California
Berkeley, California 94720

May 6, 1983

Introduction

Electrochemistry is involved to a significant extent in the present-day industrial economy. Examples are found in primary and secondary batteries and fuel cells; in the production of aluminum, chlorine, caustic soda, and other chemicals; in electroplating, electromachining, and electrorefining; and in corrosion. The electrochemical industries presently consume 6% of the total electric energy generated in the United States.[1,2] The battery industry amounts to 0.2% of the total U.S. manufacturing.[3,4] Over 3% of the total U.S. electric energy is consumed by the aluminum industry,[1,2] and the chlorine industry consumes 2% of the total U.S. electric energy.[1,2,5,6] The economic importance of corrosion is evident from the amount of money spent to protect what has been built and to replace what has been destroyed. It has been estimated[7] that corrosion prevention products amount to 3% of the U.S. electrochemical industry. The quantity of iron destroyed by corrosion lies between 25% and 33% of the total production.[8]

In spite of the economic significance of electrochemistry, engineering design procedures for electrochemical systems have not been developed as thoroughly as for mass-transfer operations such as distillation. Nevertheless, the fundamental laws governing electrochemical systems are known. The purpose of this chapter is to review the design and analysis of certain electrochemical systems in relation to these fundamental laws.

One of the difficulties in designing an electrochemical process is that there are several different kinds of reactors that can be used. These reactors can be broadly classified as either batch or continuous reactors. For example, many batteries are batch reactors, while fuel cells and many electrolysis cells are continuous reactors. Naturally, there are several different reactor geometries within each category. For example, chlorine and caustic soda are produced in any of three types of cells.[6] The diaphragm cell contains a vertical dimensionally stable anode, where chlorine is evolved, and steel screen cathodes, where hydrogen gas and hydroxyl ions are produced. The electrode compartments are separated by a porous diaphragm that allows passage of electric current. The second type of chlor-alkali cell is the membrane cell. This cell is similar to the diaphragm cell with the exception of the separator, which, in this case, is a cation exchange membrane, which inhibits

transfer of chloride and hydroxyl ions, and does not permit bulk flow of electrolyte. The third type of cell, the mercury cell, contains no diaphragm, but achieves separation of electrode products by the use of a mercury cathode, where sodium ion is reduced and forms a sodium-mercury amalgam. The amalgam is then passed to a second cell, where the amalgam is reacted with water to form sodium hydroxide, hydrogen, and pure mercury, which is recycled to the electrolyzer.

Another economically significant electrochemical reactor is the Hall-Heroult cell for the production of aluminum. This process is operated in the batch mode at high temperature (approximately 1000°C) in a bath of aluminum oxide or alumina (Al_2O_3) dissolved in fused cryolite (Na_3AlF_6), to which aluminum fluoride is added. The thermal insulation is adjusted to provide sufficient heat loss to freeze a protective coating of electrolyte on the inner walls, but not on the bottom, which must make electrical contact with the molten aluminum cathode. A crust of frozen electrolyte and alumina covers the molten electrolyte. Electric current enters the cell through carbon anodes and flows through the electrolyte, forming CO_2 at the anode and aluminum at the cathode. Steel collector bars joined to the carbon lining at the bottom conduct electric current from the cell. Some reviews of these and other industrial electrochemical processes can be found in references 6, 9 and 10.

Introduction to Design

Any chemical process requires the evaluation of various alternate routes, whether they be chemical or electrochemical. Two major tasks in designing an electrochemical reactor are first to narrow down the choices of reactor configurations and then to devise an economically optimum final design. As an example of eliminating some reactor geometries, consider metal-ion removal from dilute waste streams. In this case, it would be impractical to use two plane parallel electrodes because the reactor volume would be very high, whereas a porous electrode, with its high surface area per unit volume, would be a good candidate for this application. Porous electrodes are also more suitable for gas-evolving reactions. On the other hand, the channel configuration might be very useful for removing valuable metals, such as silver, from concentrated solutions because the

metal would be recovered directly as a sheet, rather than being incorporated in a porous structure.

After choosing some electrode configurations to evaluate, one would want to estimate the capital and operating costs and the product composition, or, in the case of a battery, the energy and power output, as a function of the feed conditions, the cell dimensions, and the operating conditions. This can sometimes be a very difficult task because there are so many phenomena that can interact, such as mass transfer, ohmic potential drop, thermodynamics, and electrode kinetics. In many cases, however, the problem can be greatly simplified by realizing which phenomena dominate the system behavior. This approach is expedient in choosing design alternatives.

In either the crude design or the final design, it is desirable to maximize profit or minimize cost. Thus, one should be aware of the various economic tradeoffs that are important in electrochemical systems. Perhaps the most obvious tradeoff is between capital and operating costs. Usually the degree of conversion is specified, and one can meet that specification either by building a large cell, with a high capital cost, or by using more power with a smaller cell. There are also other tradeoffs; for example, in a channel flow cell, one can reduce the ohmic drop and increase the mass-transfer rate by making the interelectrode gap very thin, but this will increase the pressure drop, and hence, the pumping cost. In addition, it will lead to fabrication problems and the possibility of shorts.

Governing Phenomena

If an electrochemical reactor is to be compared to an alternative, be it chemical or electrochemical, then detailed knowledge for the design and scale-up is needed. To design an electrochemical system, one needs to consider many effects, such as migration and diffusion of charged species, fluid dynamics, thermodynamics, and reaction kinetics on electrode surfaces. An additional system variable, not present in analyses of most chemical reactors, is the electric potential. It is the difference in potential between the electrode and the solution that governs which electrochemical reactions will occur. In addition, gradients of electric potential and differences in potential between phases constitute major driving forces for mass transfer and for electrochemical reactions. Thus, a knowledge of the current and potential distribution is useful in designing a reactor to carry out a

desired electrochemical reaction.

To describe mass transfer in an electrochemical system, one must consider not only ordinary diffusion, but also migration of charged species in an electric field. Because it is the flux of charged species that produces an electric current, one must include the contribution of migration to the species flux to predict correctly the current flow.

In addition to mass transfer, one must consider thermodynamics in electrochemical systems. Thermodynamics can be used to describe the properties of electrolytic solutions and their dependence on composition, temperature, and pressure. Thermodynamics also provides a framework for describing reaction equilibria, which manifest themselves in equilibrium cell potentials. Furthermore, the driving forces for irreversible processes are conveniently expressed in thermodynamic terms.

Departures from equilibrium conditions are inherent in electrochemical applications. Electrode kinetics concerns the nonequilibrium driving force, called surface overpotential, necessary to make heterogeneous electrode reactions proceed at appreciable rates.

In addition to heterogeneous reactions, there are other interfacial phenomena at electrode surfaces that can affect the current-potential behavior. The most prominent of these is the formation of a thin double layer near electrode surfaces. This double layer may be on the order of 10 to 100 Å (1 to 10 nm) in thickness.

Because there are so many interacting phenomena, it can sometimes be very difficult to design an electrochemical system. In the present age of computers, however, many problems that were intractable thirty years ago can be handled today.

In spite of the power of computers, however, it is still useful to simplify the problem if certain phenomena dominate the system behavior. For example, there are some systems where it is possible to neglect concentration variations near the electrodes. The current distribution is then determined by the ohmic potential drop in the solution and by electrode overpotentials. (The ohmic drop is simply the voltage difference that arises when current flows through the resistive solution.) Mathematically, this means that the potential satisfies Laplace's equation, and many results of potential theory,

developed in electrostatics, the flow of inviscid fluids, and steady heat conduction in solids, are directly applicable. These can be called "potential-theory problems."[11] The electrode kinetics provides boundary conditions which are usually different from those encountered in other applications of potential theory.

There are also systems where the ohmic potential drop can be neglected. The current distribution is then determined by the same principles which apply to heat transfer and nonelectrolytic mass transfer. These can be called "convective-transport problems."[11]

Some systems do not fall into either of the categories mentioned above. Fortunately, however, some of these complex systems can be treated realistically by using the computer to model the interacting phenomena.

Fundamental Equations

To calculate the current and potential distribution, which is necessary to design an electrochemical system, one needs a set of fundamental equations applicable to electrochemical systems. These equations include a description of the movement of mobile ionic species, an expression for current flow, material balances, electroneutrality, and equations from fluid mechanics. In addition, the differential equations describing the electrolytic solution require boundary conditions describing the thermodynamics and kinetics of electrode reactions.

In dilute systems, the flux of each species is given by[12]

$$\mathbf{N}_i = -z_i u_i F c_i \nabla\Phi - D_i \nabla c_i + c_i \mathbf{v} \ , \tag{1}$$

where Φ is the electrostatic potential and z_i is the number of proton charges carried by ion i. This movement is due, first of all, to the motion of the fluid with the bulk velocity $\mathbf{v}$. However, the movement of the species can deviate from this average velocity by diffusion if there is a concentration gradient, ∇c_i, or by migration if there is an electric field, $-\nabla\Phi$, and the species is charged. The migration term is peculiar to electrochemical systems or systems containing charged species.

The second and third terms on the right side of equation 1 are the usual terms required to describe diffusion and convection in nonelectrolytic systems. The species will diffuse from regions of high concentration to regions of lower concentration. The three terms on the right in equation 1 thus represent three mechanisms of mass transfer: migration of a charged species in an electric field, molecular diffusion due to a concentration gradient, and convection due to the bulk motion of the medium.

Note that equation 1 only applies to dilute solutions. A more general form of equation 1 is[12]

$$c_i \nabla \mu_i = RT \sum_j \frac{c_i c_j}{D_{ij} c_T} (\mathbf{v}_j - \mathbf{v}_i) \tag{2}$$

where μ_i is the electrochemical potential of species i. This equation must be applied to systems, such as molten salt systems, where the activity coefficients are not close to unity, or to systems where the diffusion flux of each species can be affected by more than one concentration gradient. The driving forces for diffusion and migration are both included in the gradient of the electrochemical potential in equation 2. Further details of concentrated solution theory can be found in reference 12.

After writing the appropriate flux equation, one can write an expression for the current, which is, of course, due to the motion of charged particles in an electrolytic solution.

$$\mathbf{i} = F \sum_i z_i \mathbf{N}_i \ . \tag{3}$$

Here, $\mathbf{i}$ is the current density expressed in amperes per square centimeter, and $z_i F$ is the charge per mole.

Next we need to state a material balance for any component i:

$$\partial c_i / \partial t = -\nabla \cdot \mathbf{N}_i + R_i \ . \tag{4}$$

Since reactions are frequently restricted to the surfaces of electrodes, the bulk reaction term R_i is often zero in electrochemical systems.

Finally, we can say that the solution is electrically neutral.

$$\sum_i z_i c_i = 0 . \tag{5}$$

Such electroneutrality is observed in all solutions except in the thin double charge layer near electrodes and other boundaries.

These equations provide a consistent description of transport processes in electrolytic solutions. Equations 1 or 2 state that species in the solution can move by migration, diffusion, and convection. Equation 3 merely says that the sum of fluxes of charged species constitutes an electric current. Equation 4 is a material balance for a species, and equation 5 is the condition of electroneutrality. Although the specific description may be refined, any theory of electrolytic solutions will need to consider these physical phenomena.

Note that in order to solve the equations describing the mass transfer, it is necessary to know the convective velocity $\mathbf{v}$. This velocity can be found from the equations of fluid mechanics, such as the Navier-Stokes equation

$$\rho(\partial \mathbf{v} / \partial t + \mathbf{v} \cdot \nabla \mathbf{v}) = -\nabla p + \mu \nabla^2 \mathbf{v} + \rho \mathbf{g} \tag{6}$$

and the continuity equation

$$\nabla \cdot \mathbf{v} = 0 . \tag{7}$$

Next one needs boundary conditions describing the differences in potential between phases. These boundary conditions describe the processes occurring at the electrode interface.

One process that can occur is the adsorption of ions onto the surface. (Usually anions are specifically adsorbed.) A double charge layer is formed because the ions of one sign are attracted from the solution to the adsorbed ions of the opposite sign. This attractive force, however, is balanced by thermal agitation, which tends to make the ions wander. Therefore the double charge layer has a diffuse part in the solution. That is, the charge density decreases with distance from the interface. The thickness of this diffuse layer of excess charge density is characterized by the Debye length.

$$\lambda = \left[\frac{\epsilon RT}{F^2 \sum_i z_i^2 c_{i\infty}} \right]^{1/2} . \tag{8}$$

The Debye length is typically on the order of 10 Å. The major effect of the double layer on the overall behavior of the interface is that it superimposes a capacitive effect on top of the electrode kinetics of the electrode reaction itself. This means that when the potential of the electrode is varied, the current that flows is partly due to charging the double-layer capacity, and partly due to the charge-transfer reaction. One can measure the capacitance of the double layer in several ways.[12,13] Typically[14] the double-layer capacity is 10 to 40 $\mu F/cm^2$, but this capacitance is a function of potential. The double layer is discussed further in references 12 to 16.

Although the existence of the double layer should not be neglected, it is the charge-transfer reactions at the electrodes which are usually of primary importance in electrochemical systems of practical interest. The kinetics of these reactions relate the potential driving force to the rate of reaction. Thus, a knowledge of the electrode kinetics is necessary to formulate boundary conditions for the differential equations describing the movement of ionic species.

For the purpose of assessing potential variations in a solution, it is convenient to conceive of placing reference electrodes into the solution at appropriate locations, usually just outside the diffuse double layer or in the bulk solution. Figure 1 illustrates the placement of these reference electrodes.[17] The letter s designates reference electrodes of the same kind as the working electrode, and the letter g refers to reference electrodes of a given kind. It is important to realize that a reference electrode of a "given kind" cannot be a reference electrode of *any* kind. Instead, the reference electrode must be carefully selected to be as reversible and reproducible as possible. The selection of reference electrodes is discussed in reference 12. One must also realize that a measurement made by a reference electrode of a given kind must be corrected for any liquid-junction potentials which might exist between the solution in question and that within the reference-electrode compartment (see section 40 of reference 12).

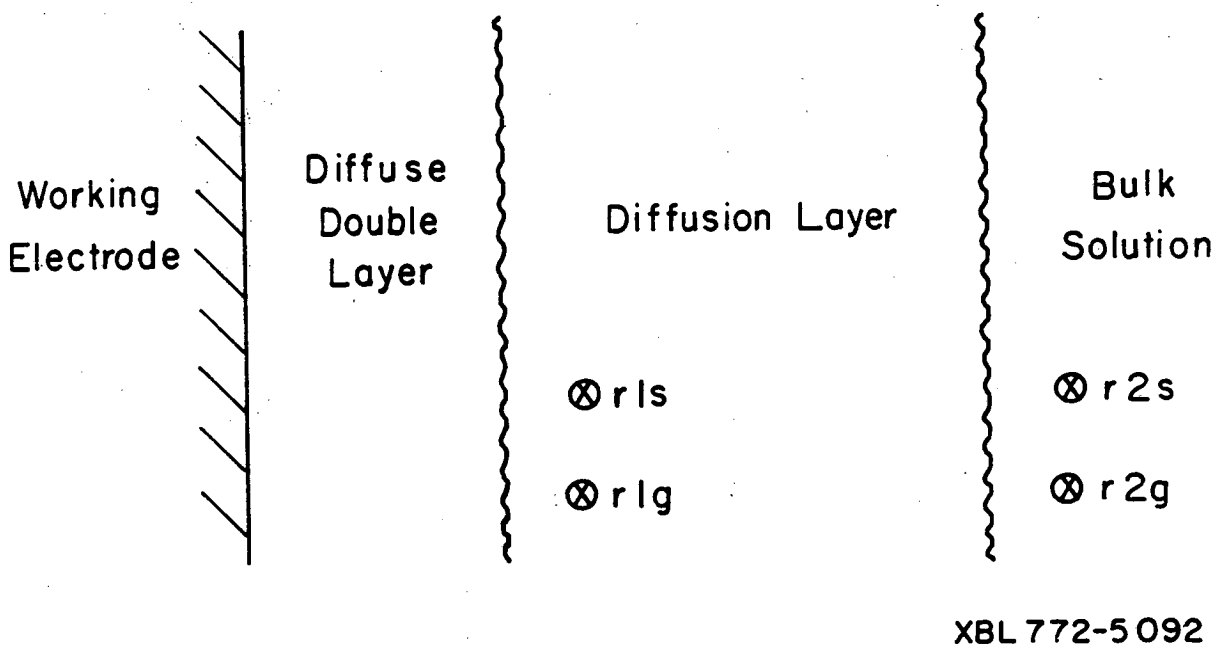

Figure 1. Reference electrodes, which may be imaginary, positioned in the bulk solution and within the diffusion layer. (17)

In the absence of concentration variations, the two reference electrodes shown in figure 1 would measure the ohmic potential drop between the two points labeled 1 and 2. In the presence of concentration variations, the potential difference between the two reference electrodes will be composed of an ohmic portion and what is called a concentration overpotential. The concentration overpotential, η_c, reflects the thermodynamic effect of the difference in concentration between the interface and the bulk solution. An additional contribution to the overall cell potential is the driving force required to make the electrode reactions proceed at appreciable rates. This surface overpotential, η_s, is defined as the potential of the working electrode relative to a reference electrode of the same kind, placed in the solution adjacent to the surface of the working electrode, but just outside the diffuse double layer. In terms of the notation of figure 1, this surface overpotential for a reaction j would be written

$$\eta_{sj} = V - V_{r1g} = V - V_{r1g} - (V_{r1s} - V_{r1g}) \tag{9}$$

or

$$\eta_{sj} = V - \Phi_o - U_{j,o} \ , \tag{10}$$

where $\Phi_o = V_{r1g}$ is the potential just outside the double layer, as measured by a reference electrode of a given kind, and

$$\begin{aligned} U_{j,o} &= V_{r1s} - V_{r1g} \\ &= \left[U_j^\theta - \frac{RT}{n_j F} \sum_i s_{ij} \ln \left(\frac{c_{io}}{\rho_o} \right) \right] - \left[U_{re}^\theta - \frac{RT}{n_{re} F} \sum_i s_{i,re} \ln \left(\frac{c_{i,re}}{\rho_o} \right) \right]. \end{aligned} \tag{11}$$

Here, the subscript re denotes the reference electrode reaction. The stoichiometric coefficient, s_{ij}, refers to species i in a reaction j, written in the form

$$\sum_i s_{ij} M_i^{z_i} \rightarrow n_j e^- \ , \tag{12}$$

where n_j denotes the number of electrons transferred, M_i refers to species i, and z_i is the charge number of species i.

For a large class of electrochemical reactions, the current density depends exponentially on the surface overpotential according to the Butler-Volmer equation

$$i_j = i_{oj}\left[\exp\left(\frac{\alpha_{aj}F}{RT}\eta_{sj}\right) - \exp\left(\frac{-\alpha_{cj}F}{RT}\eta_{sj}\right)\right], \tag{13}$$

where i_{oj} is the exchange current density for reaction j and depends on the concentrations c_i. Usually, this dependence is expressed as

$$i_{oj} = i_{oj,ref}\prod_i\left(\frac{c_{io}}{c_{i,ref}}\right)^{\gamma_{ij}}. \tag{14}$$

In equation 13, the first exponential term corresponds to the forward reaction rate for an anodic process, and the second term represents the reverse reaction rate. Note that if the anodic surface overpotential is large, the reverse reaction term can be neglected. This approximation, known as the Tafel approximation, produces a linear plot of surface overpotential *vs.* the logarithm of current density. A more thorough discussion of overpotentials can be found in references 12 and 17.

We have now introduced enough of the elements to be in a position to discuss the composition of the overall cell potential. This is due partly to the ohmic potential drop in the solution. In addition, there is a potential loss associated with the concentration variations in the solution near electrodes, which we have termed the concentration overpotential. Finally, there is the surface overpotential due to the limited rates of the electrode reactions. The sum of these is the cell potential, which can be written

$$\begin{aligned} V &= \Phi(\text{anode}) - \Phi(\text{cathode}) \qquad (15)\\ &= \Phi(\text{anode}) - \bar{\Phi}_1 + (\bar{\Phi}_1 - \bar{\Phi}_2) - \Phi(\text{cathode}) + \bar{\Phi}_2 \\ &= \eta_s(\text{anode}) + \eta_c(\text{anode}) + \Delta\bar{\Phi}_{ohm} - \eta_c(\text{cathode}) - \eta_s(\text{cathode}), \end{aligned}$$

where $\bar{\Phi}_1$ is the value that the potential adjacent to the anode would have if there were no concentration variations in the solution. The terms η_c and η_s for the cathode enter with negative signs because of the conventions that have been adopted. Since they are generally negative, they make a positive contribution to the cell potential. Thus, none of these terms, ohmic drop or overpotentials,

represents a source of energy. An example of how the various overpotentials contribute to the overall cell potential is shown in figure 2. The dotted line represents what the potential in the solution would be if all concentrations were at their bulk values.

Note that this decomposition presumes a bulk solution and a diffusion layer adjacent to each electrode. In situations where this does not prevail, such as a cell with overlapping diffusion layers, or a porous electrode, it is necessary to start over from the basic equations, but the fundamentals remain the same.

Channel Flow Cells

Channel flow between two parallel planar electrodes is used in many industrial electrochemical processes, such as metal refining, energy storage, and electro-organic synthesis. Specific examples include copper refining, some zinc-halogen energy storage cells, and the Monsanto process for conversion of acrylonitrile to adiponitrile.

Channel flow cells are very useful, since they provide continuous production, they are simple to operate and maintain, and they do not require a high capital investment.[18] In addition, the analysis of channel flow cells has been relatively well developed.[19-26]

A channel flow cell consists of two parallel plates, which serve as the anode and the cathode for electrochemical reactions. The electrolyte flows past the electrodes, and the current flow is perpendicular to the fluid flow.

In general, a thin-gap cell with multiple reactions occurring on each electrode is difficult to analyze. The electrodes cannot be treated separately, and mass transfer, thermodynamics, and the kinetics of more than one reaction must be considered simultaneously. This problem can be solved, but for design purposes, it is useful to see if any simplifications can be made. One assumption that is commonly used is that the diffusion layers are thin. In this case, the electrodes can be treated separately. This is known as the Lévêque approximation,[12,27] and it is valid as long as

$$\frac{L}{h} < 0.01\ Re\ Sc\ , \tag{16}$$

where

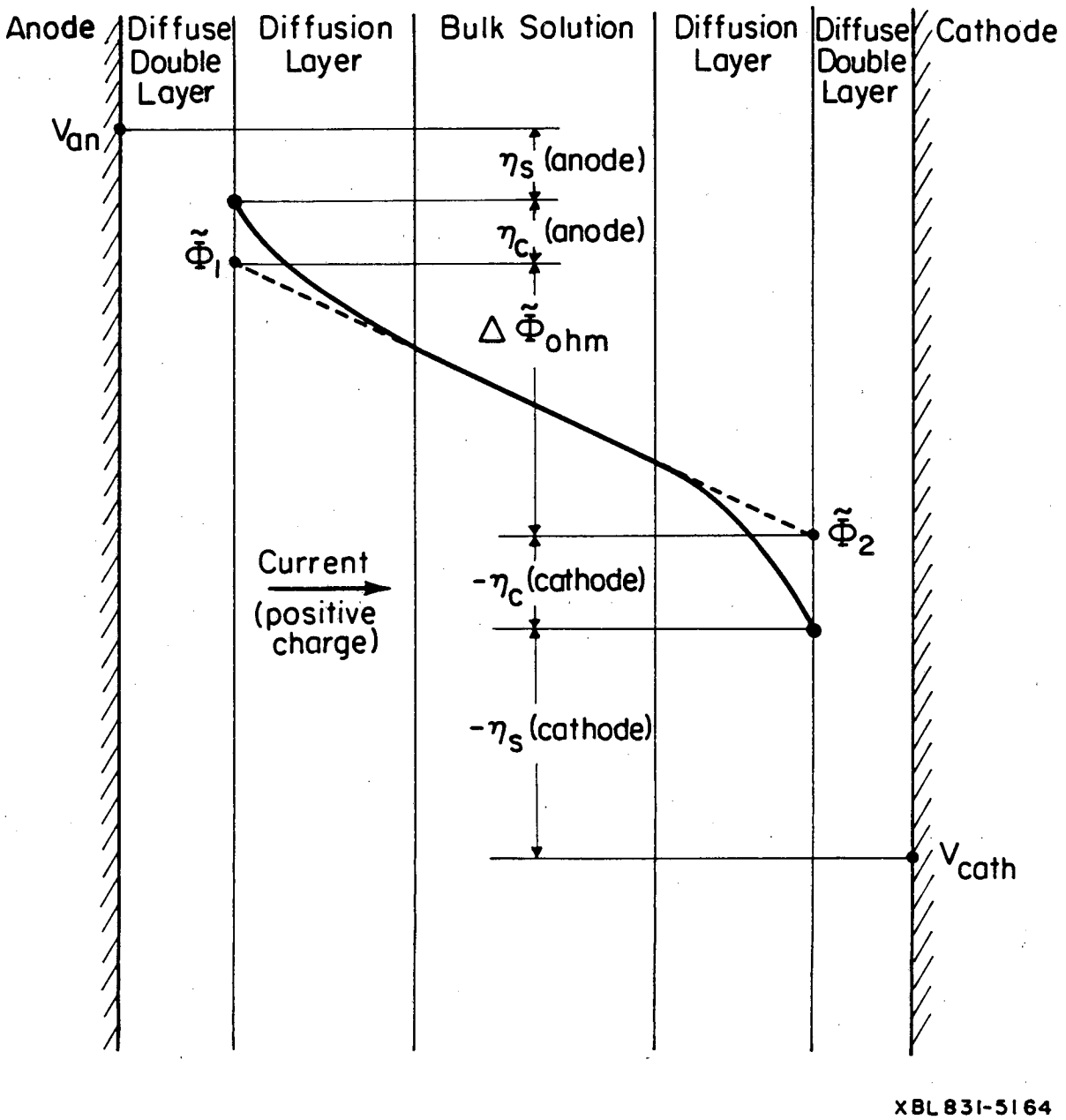

Figure 2. Overpotentials in an electrolytic cell. Solid line represents potential distribution in the absence of concentration variations.

$Re = 2 \langle v \rangle h / \nu$

$Sc = \nu / D$ (about 1000 for most aqueous systems)

L = length of electrodes

h = spacing between electrodes.

Thus we see that the thin-diffusion-layer approximation breaks down only if the electrodes are very long, the gap is very thin, or the velocity is very low.

Parrish and Newman[23] used the Lévêque approximation to obtain the current and concentration distributions in a channel flow cell. They examined the case of a metal deposition and dissolution reaction. Intuitively, one would expect that mass transfer would not be important near the front of each electrode, where the ions in solution are still unreacted. Further down the channel, however, the solution becomes depleted of metal ions. Mass transfer then begins to affect the cathodic deposition reaction. The anodic dissolution reaction, however, is not affected by the concentration of ions in the solution. Therefore, we would not expect the anodic reaction to become mass-transfer limited.

In the absence of mass transfer, the current distribution is governed by the ohmic potential drop and the reaction kinetics. This current distribution is called the secondary current distribution. If there are no kinetic limitations, however, the current distribution is called the primary distribution. To calculate the primary current distribution, one would solve Laplace's equation for the potential, assuming that the potential adjacent to each electrode is held at a constant value. For two electrodes embedded in planar channel walls, the primary current density is infinite at the electrode edges. The secondary current distribution is similar to the primary distribution, but it is more uniform because there are kinetic limitations. Therefore, the current density is not infinite anywhere, but it is still higher at the electrode edges.

If mass transfer dominates the current distribution, on the other hand, the current density is high only at the front of the electrode, and it decreases with distance down the channel.

For an anodic dissolution reaction, one would expect that mass transfer would not be important. Therefore, the current distribution should resemble the secondary current distribution. Parrish and Newman found that this is indeed the case. The cathodic current distribution, however,

should behave like a secondary current distribution near the front of the electrode, but like a mass-transfer limited current distribution near the back. In fact, Parrish and Newman's numerical results show maxima in the cathodic current densities. These maxima arise from a compromise between the secondary current distribution and the mass-transfer-limited current distribution.

Throughout their analysis, Parrish and Newman assumed a single reaction at each electrode. Very often, this simplifying assumption is valid.[28] Occasionally, however, multiple reactions must be considered.[19,20,21,29] The assumption of a single reaction may be checked by identifying a single parameter which characterizes the manner in which a side reaction tends to obscure the limiting-current plateau for a main, or desired, reaction.[29] It is the magnitude of the side reaction relative to the main reaction at potentials in the neighborhood of the limiting-current plateau which is important.

Figure 3 illustrates this concept for the example of copper deposition as the main reaction and hydrogen evolution as the side reaction. The solid line, labeled "Main Cathodic Reaction," is the current-potential curve of interest. The curves in the figure are plots of the potential difference, $V - \tilde{\Phi}_o$, *vs.* the logarithm of the current density, where V is the electrode potential, and $\tilde{\Phi}_o$ is the potential in the solution just outside the double layer, as measured by a reference electrode of the same kind as the main reaction. Note that the potential difference $V - \tilde{\Phi}_o$ is related to the surface overpotential by equation 10,

$$\eta_{sj} = V - \tilde{\Phi}_o - U_{j,o} \ , \tag{10}$$

where $U_{j,o}$ is defined by equation 11.

Figure 3 shows the following six curves:

1. Tafel Approximation of Main Anodic Reaction (copper dissolution)
2. Tafel Approximation of Side Anodic Reaction (production of hydrogen ions)
3. Tafel Approximation of Main Cathodic Reaction (copper deposition)
4. Tafel Approximation of Side Cathodic Reaction (hydrogen evolution)
5. Main Cathodic Reaction Limiting Current
6. Main Cathodic Reaction (copper deposition)

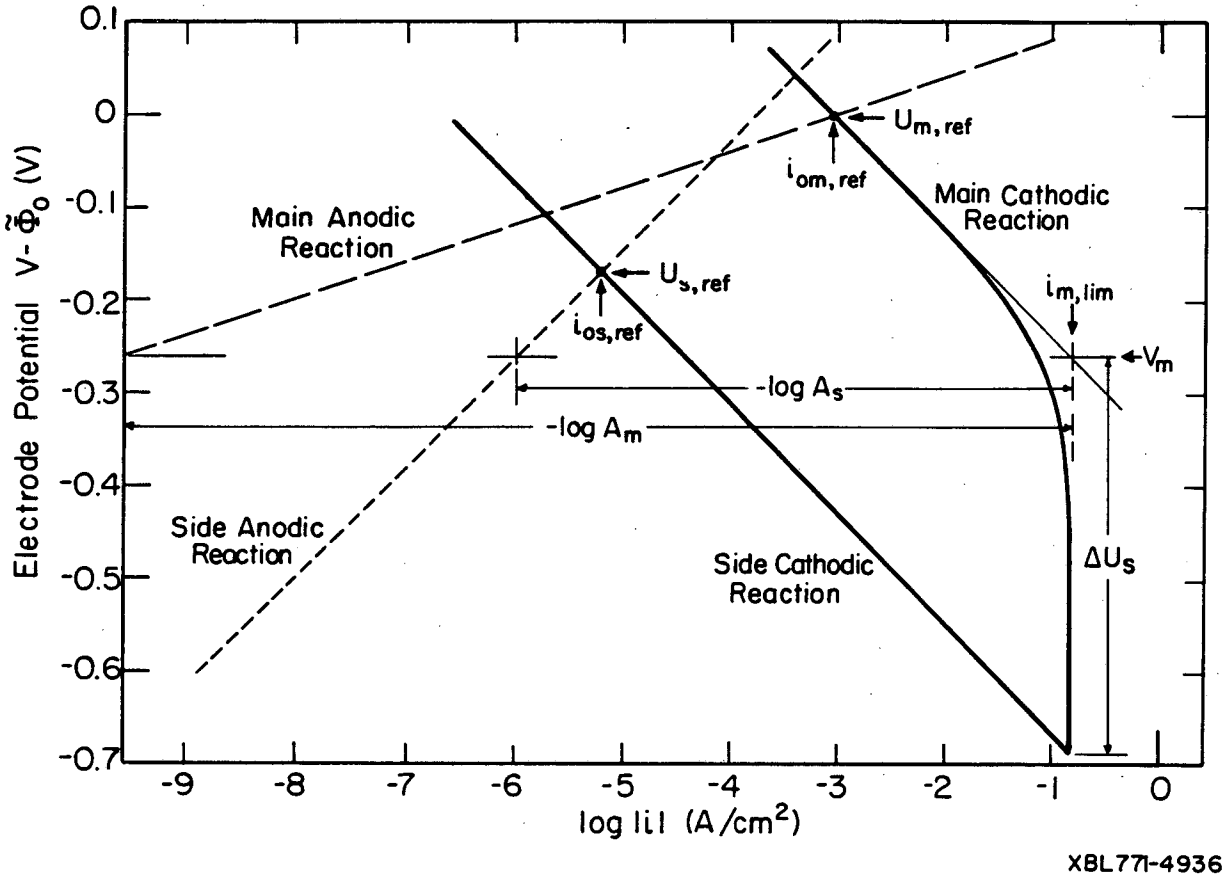

Figure 3. Qualitative sketch of the current-potential curves for a main and a side reaction showing some of the parameters defined in the text. (17)

The heavy line for the main cathodic reaction has two asymptotes: at high $|V - \tilde{\Phi}_o|$, the reaction is mass-transfer controlled (curve 5); at low $|V - \tilde{\Phi}_o|$, the reaction is kinetically controlled (curve 3).

The Tafel approximation is applied to the cathodic reactions, since it is unlikely that the backward terms in the Butler-Volmer equation are important in the neighborhood of the limiting-current plateau, where $-\eta_{s,m}$ is large. The anodic reactions are plotted as Tafel lines to illustrate that the limiting-current plateau is not affected by either anodic reaction. Although the Tafel approximation is not valid near $i = i_o$, we are interested in the neighborhood of the limiting-current plateau, which is far from i_o. Therefore, we only examine the portion of the Tafel curve near the limiting-current plateau, where the backward terms in the Butler-Volmer equation can be neglected.

As long as there are no mass-transfer limitations, the plot of $V - \tilde{\Phi}_o$ *vs.* $\log |i|$ will remain linear. Note that the solid line for the main cathodic reaction does start to bend over as mass transfer comes into play. The side cathodic reaction, hydrogen evolution, however, has no mass-transfer limitations because hydrogen evolution occurs from a solution with excess hydrogen ion in the supporting electrolyte.

To plot a Tafel line, one needs not only the slope, but also the value of $V - \tilde{\Phi}_o$ at a single current density, i. If this current density is chosen as the exchange current density at the reference concentrations, then

$$V - \tilde{\Phi}_o = U_{m,ref} \ , \tag{17}$$

where $U_{m,ref}$ is given by

$$U_{m,ref} = U_m^\theta - U_{re}^\theta - \frac{RT}{n_m F} \sum_i s_{im} \ln \left(\frac{c_{i,ref}}{\rho_o} \right) + \frac{RT}{n_{re} F} \sum_i s_{i,re} \ln \left(\frac{c_{i,re}}{\rho_o} \right) . \tag{18}$$

The Tafel approximation can also be written for the main reaction in the anodic direction. Again, at $i = i_{om,ref}$, $|V - \tilde{\Phi}_o|$ is $U_{m,ref}$. In fact, the anodic and cathodic Tafel lines, for any reaction j, intersect at $i_{oj,ref}$ and $U_{j,ref}$, if the surface concentrations are at their reference values. Therefore, for any reaction j, if one knows the exchange current densities, $i_{oj,ref}$, and the anodic and cathodic transfer coefficients, α_{cj} and α_{aj}, one can plot lines similar to those shown in figure 3.

The parameters A_m and A_s, also shown in figure 3, characterize the magnitude of the anodic part of a reaction, at the electrode potential for which the main reaction is beginning to reach the limiting current. This parameter is defined,[29] for a reaction j, as

$$A_j = \left| \frac{i_{oj,ref}}{i_{m,lim}} \right|^{1 + \alpha_{aj}/\alpha_{cj}} \exp\left(\frac{\alpha_{aj} F}{RT} \Delta U_j \right) . \tag{19}$$

It should be noted that, if the surface concentrations are not at the reference values, the Tafel lines will be shifted. For example, if the concentration of dissolved hydrogen is less than $c_{H_2,ref}$, then the Tafel line for the anodic side reaction will be shifted to the left. The exact placement of this line, in this case, however, does not affect the length of the limiting-current plateau for the main reaction. In fact, neither anodic reaction affects the length of the limiting-current plateau. Thus, since the limiting-current region is of greatest interest, the anodic reactions are not important.

The electrode potential, V_m, for which the main reaction is beginning to reach the limiting current is, in the absence of an ohmic potential drop, approximately equal to

$$V_m = U_{m,ref} - \frac{RT}{\alpha_{cm} F} \ln\left(\frac{-i_{m,lim}}{i_{om,ref}} \right) . \tag{20}$$

At the potential defined by equation 20, the current density for the side reaction divided by the limiting current density for the main reaction is proportional to $\exp(-\alpha_{cs} F \Delta U_s / RT)$, where

$$\Delta U_s = U_{m,ref} - U_{s,ref} - \frac{RT}{\alpha_{cs} F} \ln\left(\frac{i_{os,ref}}{-i_{m,lim}} \right) + \frac{RT}{\alpha_{cm} F} \ln\left(\frac{i_{om,ref}}{-i_{m,lim}} \right) \tag{21}$$

corresponds to the length of the limiting-current plateau, as shown in figure 3. The parameter ΔU_s shows that both the exchange current density and the open-circuit potential determine the relative significance of a side reaction. If the exchange current density is very small or the open-circuit potential is quite negative, ΔU_s will be large, and the side reaction will not obscure the limiting-current plateau.

Cell Optimization

The goal in designing any reactor is to maximize the profit or to minimize the total cost by making an appropriate choice of operating variables and cell dimensions. Naturally, there are constraints, such as mass-transfer and current-potential relationships, as well as feed and product specifications. Usually, however, there are few enough constraints that there is enough flexibility to perform a cost minimization.

An example of the tradeoff between capital and operating costs in a fuel cell has been discussed by Newman.[30] Ibl and his co-workers[31-33] have also treated the design and optimization of various electrochemical systems. Alkire *et al.*[34] have discussed the optimization of electrochemical systems having many variables. We shall discuss here the example of optimization of potential and hydrogen utilization in an acid fuel cell.

A fuel cell for commercial power generation consists of a device to reform a hydrocarbon fuel to yield hydrogen and an electrochemical reactor, where this hydrogen is combined with oxygen from the air to produce water vapor and electric power. In this example, we shall perform a simplified cost analysis, where only the capital costs and the fuel costs will be included. The fuel cost, denoted C_f, will include all operating costs which can be associated with or set proportional to the consumption of fuel. Thus, the reformer costs will be included in C_f. The tradeoff between capital and operating costs results because there is an optimum fuel utilization beyond which the increase in electrode area costs more than can be justified by the increase in electric power produced.

To perform the optimization, one must first write an expression for the cost to be minimized. In this example, we shall write the cost in terms of the hydrogen utilization u and the cell potential V where utilization is defined as the fraction of the hydrogen in the feed that is consumed in the electrochemical reactor. To write the cost in terms of only the variables u and V, one needs to know how the cell potential depends on current density and gas composition. Once the cost is written in terms of u and V, the optimization is performed by simply setting the derivatives of the cost with respect to u and V equal to zero, and solving for u and V.

To calculate the relationship among cell potential, current density and gas composition, one can assume that the air cathode obeys Tafel kinetics. At the hydrogen electrode, on the other hand, the surface overpotential is negligible, and the Nernst equation applies, where the anode potential differs from the potential of the adjacent hydrogen reference electrode mainly because the hydrogen partial pressure differs from the reference pressure of 1 atm. Finally, one can calculate the ohmic potential drop within the cell and combine the three equations to obtain the relationship among cell potential, current density and gas composition,

$$V = U' + \frac{RT}{F} \ln \left(\frac{p_{O_2} \, p_{H_2}^{\,1/2}}{I} \right) - R' \, I \, . \tag{22}$$

The partial pressures of oxygen and hydrogen appearing in equation 22 are at the catalyst layers and must be obtained from the values in the flowing streams by allowance for the gas-phase mass-transfer resistance through the inert gas in the electrode substrates. These partial pressures are then substituted into equation 22 to obtain the desired current-potential relationship.

Next, one needs an expression for the total cost. In this example, the total cost is the fuel cost plus the capital cost. Let C_f be the value of a unit of hydrogen in the feed, and $K_u C_f$ be the value of hydrogen in the exit fuel stream after a utilization u, where C_f is expressed in \$/coulomb. Let the capital costs be expressed by C_a, having units of \$/s-cm^2, based on superficial electrode area. C_a is obtained by multiplying the total capital cost (\$/cm^2) by a factor such as 0.3 yr^{-1}, representing the effect of interest, depreciation, and taxes. Components with a five-year life and a 10% interest rate might give rise to this factor. The total cost can now be expressed as

$$\frac{\text{cost}}{\text{time}} = C_f \, 2FF_a X_{H_2}^{o} - C_f K_u \, 2FF_a X_{H_2}^{exit} + C_a A_{tot} \, , \tag{23}$$

where F = Faraday's constant, 96,487 C/equiv

F_a = flow rate of inerts on anode side, mol/s

$X_{H_2}^{exit}$ = ratio of moles of H_2 to moles of inerts in the exit stream

$X^o_{H_2}$ = ratio of moles of H_2 to moles of inerts in the feed stream

A_{tot} = superficial electrode area, cm^2.

The first term on the right is the cost of the hydrogen feed stream, the second term is the resale value of the hydrogen exit stream, and the last term is the capital cost. We are concerned with minimizing the cost per unit of electric energy, which is the ratio of the cost per unit time to the electric power produced, where

$$\text{Power} = P = \int_0^{A_{tot}} V\, I\, dA\ . \tag{24}$$

Here, I is the superficial current density, expressed in A/cm^2. As a step toward writing the total cost in terms of u and V, we can relate the flow rate and consumption of hydrogen to the electric current by Faraday's Law

$$2FF_a(X^o_{H_2} - X_{H_2}) = 2FF_a X^o_{H_2} u' = \int_0^A I\ dA\ , \tag{25}$$

where u' denotes the value of the utilization u for a local mole ratio X_{H_2} of hydrogen. Now we can write the total area as

$$A_{tot} = 2FF_a X^o_{H_2} \int_0^u \frac{du'}{I}\ , \tag{26}$$

and the electric power from equation 24 becomes

$$P = 2FF_a X^o_{H_2} \int_0^u V\ du'\ . \tag{27}$$

By means of these relationships, the power cost takes the form

$$C_e = \frac{\left[C_f - C_f K_u (1-u) + C_a \int_0^u \frac{du'}{I} \right]}{\int_0^u V\ du'}\ . \tag{28}$$

This equation has been written so that the extensive quantities – power required, electrode area A_{tot}, and flow rate of the fuel stream – have been eliminated in favor of the utilization u, an intensive variable.

We shall restrict ourselves here to the case where the cell potential V is a constant for all values of the utilization. Now we can set the derivatives of the power cost in equation 28 with respect to u and V equal to zero. The differentiation with respect to u gives, after some manipulation,

$$\frac{C}{I} = \frac{1-K_u}{u} + \frac{C}{u}\int_0^u \frac{du'}{I} + (1-u)\frac{dK_u}{du}, \tag{29}$$

where $C = C_a/C_f$ is the ratio of the capital cost to the fuel cost and has the units of A/cm^2. The differentiation with respect to V gives

$$1-K_u(1-u) + C\int_0^u \frac{du'}{I} = -VC\int_0^u \left(\frac{\partial I}{\partial V}\right)_u \frac{du'}{I^2}. \tag{30}$$

The results of this optimization show that when depleted hydrogen can be sold at cost, that is, $K_u = 1$, it is economical to operate with the richest fuel and air streams available, as expected. Thus the optimum utilization obtained from equation 29 is $u = 0$. Substituting this into equation 30 gives

$$-\frac{\partial V}{\partial I}\left(1 + \frac{I}{C}\right) = \frac{V}{I}. \tag{31}$$

This equation, when coupled with the current-potential relationship, gives the optimum current density or cell potential. For C, the ratio of capital to fuel cost, approaching infinity, equation 31 says that the power maximum, where $dVI/dI = 0$, is the optimum. As fuel costs become more important and C decreases, optimum operation is at a current density below (and a potential above) the power maximum. The limit $K_u = 1$ will give the most favorable power cost,

$$C_e = \frac{C_f}{V}\left(1 + \frac{C}{I}\right). \tag{32}$$

The other extreme is $K_u = 0$, where waste hydrogen has no value. This will be the worst case and will yield the highest optimum utilization, for a given cost ratio C.

Porous Electrodes

1. Introduction

In the discussion above we have considered a flow channel as a possible reactor configuration. We wish now to focus attention on porous electrodes as another class of electrochemical reactors.

Porous electrodes can be used in flow-through configurations as in fuel cells, redox energy storage systems, and chemical reactors or in closed configurations as in many primary and secondary batteries. Thus, porous electrodes find potential applications as electrochemical reactors in a variety of areas. Flow-through porous electrodes are reviewed by Newman and Tiedemann.[35] The mass transfer of reacting species within the fixed bed and the ohmic potential variation throughout the bed are treated in detail. A second review article treats porous electrodes with regard to battery applications.[36] A literature survey is given in each review.

Two distinguishing features of porous electrodes are the intimate contact of the electrode with the solution (and possibly a gaseous phase) and the high surface area to volume ratio that can be obtained. The high surface area to volume ratio is important to applications where the intrinsic rate of the heterogeneous, electrochemical reaction is slow. In processes using double-layer adsorption, the high surface area is again important. Dilute reactants in solution require the close proximity of solution and electrode to enhance mass transfer to the electrode surface. In battery or fuel-cell applications, porous electrodes offer a means for storing the soluble reactants in close proximity to the electrode surface. For non-conducting reactants of low solubility, another solid phase (as in batteries) or gas phase (as in fuel cells) may be incorporated into the system.

Flow-through porous electrodes could find applications in the area of metal processing. This includes the purification, electrowinning, and possibly electroplating of aluminum, copper, magnesium, sodium, manganese, nickel, gold, silver, and chromium. The electrorefining of aluminum

from an aluminum-manganese alloy might involve a flow-through porous anode in order to prevent the dissolved manganese from reaching the cathode. Solutions too dilute to treat with electrowinning processes may be treated with a flow-through porous electrode. Dilute aqueous metal removal and recovery of copper,[37] silver,[38] and mercury[39] have been studied in fixed-bed, flow-through porous electrodes. Copper was recovered from feed streams of 667 ppm with effluent concentrations less than 1 ppm, with simultaneous production of a concentrated stream of 47,660 ppm. Copper recovery has also been investigated in fluidized-bed reactors.[40,41] Gold can readily be recovered from plating baths which have deteriorated, and streams from processing photographic emulsions can be reduced to less than 1 ppm silver. Mercury contamination in brine solutions has been reduced to concentrations as low as 5 ppb from feed streams of 50 ppm. Reduction of contaminants usually requires processing of large volumes of dilute solutions. For metal removal, consideration must be made for the periodic removal of material from the matrix. Oxidation of organic contaminants, however, can proceed with no retention of solids.

The use of porous electrodes in electro-organic syntheses may provide an economical alternative to other chemical routes. The electrochemical synthesis may give higher yields under less severe operating constraints. The ability to control the electrode potential allows optimization for a particular reaction product, while minimizing side reactions or multiple products. A bibliography of electro-organic syntheses has been recently compiled by Swann and Alkire.[42]

Energy storage and conversion systems may use flow-through porous electrodes. Flow-redox systems, zinc-chlorine hydrate storage systems, and fuel cells are some examples. It has also been shown that the performance of some primary or secondary batteries could be enhanced by a fresh supply of electrolyte.[43,44] A promising zinc-bromine secondary battery system uses a flowing electrolyte.

Flow-through porous electrodes also find applications in fundamental studies. Appel and Newman[45] apply a limiting current method for the measurement of mass-transfer coefficients at very low Reynolds numbers. Fedkiw and Newman[46] summarize mass-transfer results of several workers. The results are correlated by a dual-sized, straight-pore model for the bed's pore volume.

2. Governing Equations

The many potential applications of porous electrodes warrant the need for a mathematical description of the system. One can then scale-up a system or predict the result of a change in operating parameters. This modeling can lead to designs that optimize or maximize the desired process. Less detailed modeling can be a guide in screening various alternatives such as newly proposed battery systems. It is important, then, to develop guidelines as to the behavior of porous electrodes.

Porous electrodes are inherently different from planar electrodes due to the intimate contact of the solution and matrix phases. Here the current flows within the matrix and the solution phases, and exchanges between the matrix and solution nonuniformly throughout the bed. An electrical analog that can help picture the inherent complications is seen in figure 4. This figure shows two porous electrodes operating as an electrolytic cell. The subscripts 1 and 2 refer to the matrix and solution phases respectively. Subscripts a and c refer to the anode and cathode, and R_s represents the resistance due to the separator. When current flows through the porous electrode, the electrical double-layer capacity (represented by C_d) is charged. This is a net flow of current through the solution causing a change in solution composition near the interface. In parallel to this process, net current flows via a faradaic reaction where R_F represents the charge-transfer resistance of the electrochemical reaction. These processes occur nonuniformly throughout the volume of the porous bed. It is cautioned that this figure is meant to serve as a guide in thinking about the distribution of reactions in porous electrodes, but is not a substitute for modeling the porous electrode with the appropriate governing equations. Mass transfer of reacting species, for example, is not considered in the electrical analog.

The mathematical description of porous electrodes assumes a macrohomogeneous system. The porous bed is represented as the superposition of two continua, a matrix and a solution. The actual geometric detail of the bed is ignored. Average physical parameters such as porosity and surface area are used. This type of analysis leads to a volume-averaged approach in the governing differential equations.[47,48]

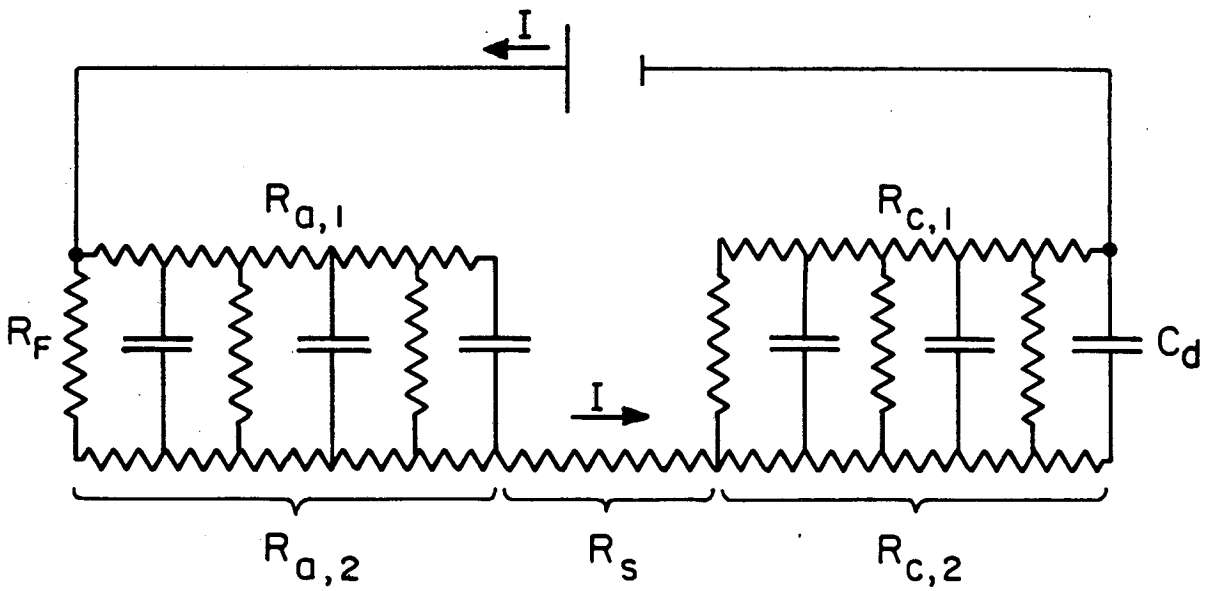

XBL 833-5452

Figure 4. Simplified electrical analog of a porous anode and cathode (subscripts a and c respectively) showing the resistance in the matrix phases (subscript 1) and solution phases (subscript 2). Also shown is the faradaic charge transfer resistance (R_F), electrical double-layer capacity (C_d), and separator resistance (R_S).

A schematic of a section of a porous bed is shown in figure 5. The volume-averaged material balance[48] of a species i within a flooded porous bed in the absence of homogeneous chemical reactions takes the form (compare equation 4)

$$\frac{\partial(\epsilon c_i)}{\partial t} = a j_{in} - \nabla\cdot\mathbf{N}_i. \tag{33}$$

Here three different averages are used. ϵ is the porosity or void volume fraction. a is the specific interfacial area (surface area of pore walls per unit volume of bed). c_i is the concentration averaged over the volume of solution in the pores. ϵc_i is then the superficial concentration averaged over the bed volume (matrix plus pores). j_{in} is the normal component of the pore wall flux of species i into the solution relative to the velocity of the pore wall, averaged over the interfacial area. $\mathbf{N}_i$ is the average flux of species i in the pore solution averaged over the cross-sectional area of the pore plus matrix.

With the flux $\mathbf{N}_i$ referenced to the cross-sectional area of the pore plus matrix, the superficial current density $\mathbf{i}_2$ in the solution phase is given as

$$\mathbf{i}_2 = F\sum_i z_i \mathbf{N}_i. \tag{34}$$

Similarly, $\mathbf{i}_1$, the current density in the matrix phase, is defined to refer to the superficial area and not to the area of an individual phase.

The matrix and solution phases are taken to be electrically neutral. For the solution, then,

$$\sum_i z_i c_i = 0. \tag{35}$$

We have assumed that the electrical double layer at the matrix pore interface is a small volume compared to our averaging volume. This assumption may break down for very dilute solutions and high-surface-area electrodes. Electroneutrality requires that the divergence of the total current density $(\mathbf{i}_1 + \mathbf{i}_2)$ is zero; charge leaving the matrix must enter the solution. Thus,

$$\nabla\cdot\mathbf{i}_1 + \nabla\cdot\mathbf{i}_2 = 0. \tag{36}$$

A combination of equations 33, 34, and 35 gives

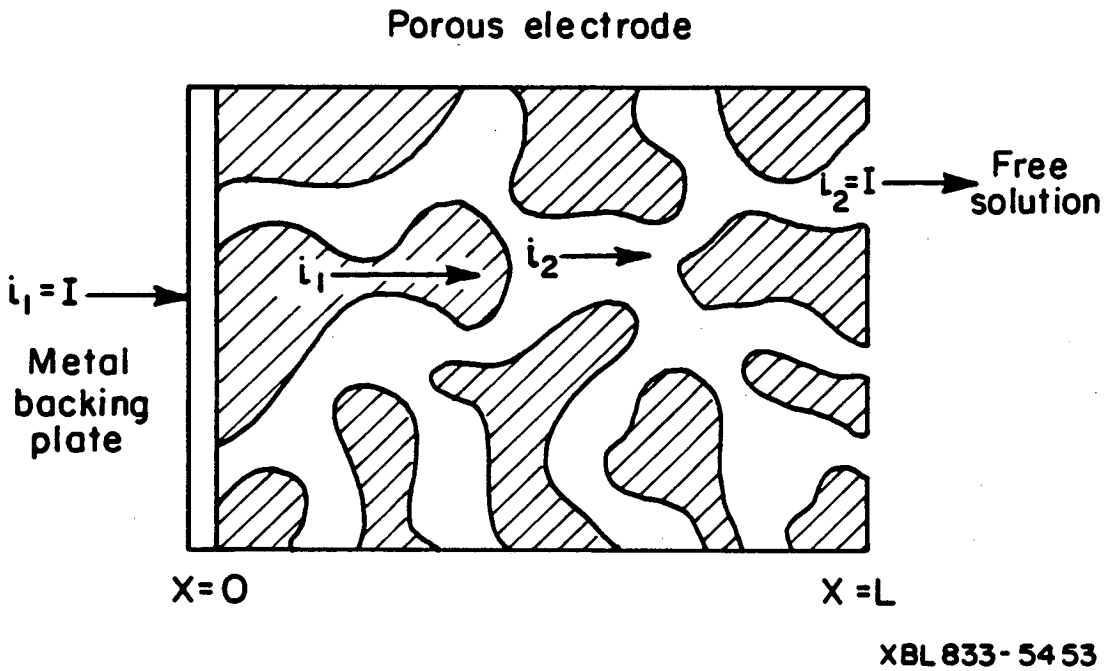

Figure 5. Schematic of a one-dimensional porous electrode.

$$\nabla\cdot\mathbf{i}_2 = aF\sum_i z_i j_{in} = ai_n \ , \tag{37}$$

where i_n is the average transfer current density from the matrix to the solution phase. $\nabla\cdot\mathbf{i}_2$ is the transfer current per unit volume of the electrode (A/cm^3) and is positive for anodic currents. For a single electrode reaction represented as

$$\sum_i s_i M_i^{z_i} \rightarrow ne^-, \tag{38}$$

Faraday's law becomes

$$aj_{in} = -\frac{as_i}{nF} i_n = -\frac{s_i}{nF}\nabla\cdot\mathbf{i}_2 \ . \tag{39}$$

Substitution into equation 33 and neglect of double-layer charging yield

$$\frac{\partial(\epsilon c_i)}{\partial t} = -\nabla\cdot\mathbf{N}_i - \frac{s_i}{nF}\nabla\cdot\mathbf{i}_2 \ . \tag{40}$$

A kinetic polarization equation relating the local rate of reaction (transfer current density) to the surface concentrations and interfacial potential drop is needed. For the porous electrode, equation 13 becomes

$$\nabla\cdot\mathbf{i}_2 = ai_0\left[\exp\left(\frac{\alpha_a F}{RT}\eta_s\right) - \exp\left(\frac{-\alpha_c F}{RT}\eta_s\right)\right] \tag{41}$$

Porosity changes can be taken into account by a solid-phase material balance for a single electrode reaction:

$$\frac{\partial\epsilon}{\partial t} = -A_0\nabla\cdot\mathbf{i}_2 \ , \tag{42}$$

where

$$A_0 = -\sum_{\substack{solid\\phases}} \frac{s_i M_i}{\rho_i nF} \ . \tag{43}$$

Transport processes are needed to complete our description. Ohm's law for the matrix phase is

$$\mathbf{i}_1 = -\sigma\nabla\Phi_1, \tag{44}$$

where σ is an effective matrix conductivity dependent on the composition of solid phases, the manner in which the grannules of the conducting phases are connected together, and the volume fraction of conducting phase or phases.

For a dilute electrolytic solution in the pores, the flux of a mobile solute can be attributed to diffusion, dispersion, migration, and convection (compare equation 1):

$$\frac{\mathbf{N}_i}{\epsilon} = -(D_i + D_a)\nabla c_i - z_i u_i F c_i \nabla\Phi_2 + \frac{\mathbf{v}\, c_i}{\epsilon}, \tag{45}$$

where u_i is a corrected ionic mobility and D_i is an ionic diffusion coefficient corrected for the tortuosity of the pores. D_a represents the effect of axial dispersion. A discussion of the effect of axial dispersion on the average mass-transfer coefficient is found in the review article by Newman and Tiedemann;[35] see also Fedkiw and Newman.[49] The current density in the solution phase can now be represented by

$$\mathbf{i}_2 = -\kappa\nabla\Phi_2 - \epsilon F \sum_i z_i D_i \nabla c_i \ , \tag{46}$$

where $\kappa = \epsilon F^2 \sum_i z_i^2 u_i c_i$. The second term in equation 46 represents the diffusion potential. As a consequence of electroneutrality, convection and dispersion make no contribution to the current density.

We should also recognize here that other forms of the transport equations may be necessary to describe a system. The appropriate equations for a concentrated binary electrolyte are given in Newman and Tiedemann.[36] Two binary molten salts are treated by Pollard and Newman.[50] When necessary, the full multicomponent transport equations can be used. (Compare the discussion of equation 2.)

In summary, the equations presented above have been found to describe adequately porous electrodes in many cases. A certain level of complexity is necessary in order to treat the simultaneous interaction of the physical processes. Equations 33, 34, 35, and 45 govern the transport, conservation, and electrical neutrality in the solution phase. Equation 44 covers the transport in the matrix phase. Equations 36 and 41 couple the species in the bulk phase to the electrochemical

processes occurring at the interface. These equations are normally considered boundary conditions in systems not involving porous electrodes, but here they are applied throughout the volume of the bed.

Let us now illustrate an important design principle for flow-through porous electrodes.[35,37] Consider the case of reducing a species i at the limiting current in an excess of supporting electrolyte. Equation 33 becomes

$$\frac{dN_i}{dx} = aj_{in} \tag{47}$$

for a one-dimensional, steady-state material balance. In the absence of migration in an electric field for the reacting species, the superficial flux of species i in the direction of the superficial fluid velocity is (from equation 45)

$$N_i = -\epsilon(D_i + D_a)\frac{dc_i}{dx} + c_i v. \tag{48}$$

The local flux to the wall is given by a local mass-transfer coefficient k_m such that

$$j_{in} = k_m(c_{io} - c_i) = -k_m c_i, \tag{49}$$

where the wall concentration c_{io} has been set equal to zero at limiting current. Substitution of equations 48 and 49 into the continuity equation 47 gives

$$v\frac{dc_i}{dx} = \epsilon(D_i + D_a)\frac{d^2c_i}{dx^2} - ak_m c_i. \tag{50}$$

Equation 50 governs the concentration distribution of species i throughout the reactor. It is solved subject to the Danckwerts,[51] Werner and Wilhelm[52] boundary conditions for the concentration of species i at the inlet ($x = 0$) and the outlet ($x = L$) of the reactor. This formulation assumes that an inert packing extends from the active portion of the bed in both the upstream and downstream directions. A result of the constraints that the concentration of species i cannot increase without bounds and that the concentration and flux should be continuous is that

$$\frac{dc_i}{dx} = 0 \quad at \quad x = L\,. \tag{51}$$

For the upstream boundary condition, an inlet concentration of c_0 and continuous concentration and flux give

$$c_0 v = c_i v - \epsilon(D_i + D_a)\frac{dc_i}{dx} \quad at \quad x = 0 . \tag{52}$$

Under this condition, the concentration at the inlet of the bed will be less than c_0 because some of the reactant will have diffused ahead to the active portion of the bed. The solution to equation 50 subject to boundary conditions 51 and 52 is

$$\theta = \frac{e^{-y/B} + \frac{D'}{B^2}e^{By/D'}\exp\left[-\alpha L\left(\frac{1}{B} + \frac{B}{D'}\right)\right]}{B + \frac{D'}{B^2}(1 - B)\exp\left[-\alpha L\left(\frac{1}{B} + \frac{B}{D'}\right)\right]} , \tag{53}$$

where we have introduced the quantities

$$\begin{aligned} &\theta = \frac{c_i}{c_0}, \quad y = \frac{ak_m x}{v}, \quad D' = \frac{\epsilon a k_m}{v^2}(D_i + D_a) , \\ &B = \frac{1 + \sqrt{1 + 4D'}}{2} , \quad \text{and } \alpha = ak_m/v. \end{aligned} \tag{54}$$

Note that equation 53 simply reduces to

$$\begin{aligned} c_i &= c_0 e^{-\alpha x} \\ \text{or } \theta &= e^{-y} \end{aligned} \tag{55}$$

when the effects of axial dispersion and diffusion are ignored.

Substitution of Faraday's law for the local flux to the wall in equation 49 governs the behavior of the superficial current density in the solution. Equation 50 becomes

$$v\frac{dc_i}{dx} = \epsilon(D_i + D_a)\frac{d^2c_i}{dx^2} - \frac{s_i}{nF}\frac{di_2}{dx} . \tag{56}$$

For an upstream counterelectrode, the current density i_2 must go to zero at the back of the electrode as all the current has been transferred to the matrix and current collector. Using this boundary condition and integrating equation 56 give

$$v(c_i - c_L) = \epsilon(D_i + D_a)\frac{dc_i}{dx} - \frac{s_i}{nF}i_2 , \tag{57}$$

where the subscript L refers to the exit of the reactor. Ohm's law for the solution (equation 46) is taken as

$$i_2 = -\kappa\frac{d\Phi_2}{dx} . \tag{58}$$

The diffusion potential has been ignored here, a good assumption when an excess of supporting electrolyte is present. Integration of equation 58 subject to equations 57 and 54 gives the local variation of potential through the bed. This result is expressed as

$$\Phi_2(L) - \Phi_2(0) = \frac{nFvc_0}{s_R\kappa}\frac{v}{ak_m}\left[B^2\theta_L e^{\alpha L/B} - \frac{D'}{B} - (\alpha L + 1 + D')\theta_L\right]. \tag{59}$$

Figure 6 shows the nature of the potential variation through the electrode bed. The potential in the matrix is constant through the length of the bed if the matrix conductivity is very high. The ohmic potential drop in the solution causes the variation in solution potential. The potential driving force at the back of the electrode $\Phi_1 - \Phi_2(L)$ must be large enough to insure limiting current, while the potential difference at the front of the electrode must not be large enough to have secondary reactions, such as hydrogen evolution. Thus, we have a maximum allowable ohmic potential drop in our reactor. As the bracketed quantity in equation 59 is of order unity, the coefficient of this quantity represents the magnitude of the potential variation in the porous bed. Thus we see that, for given values of c_0 and κ, side reactions limit the maximum flow rate through the bed. Since v/ak_m represents the order of magnitude of the distance through the reactor where the reaction occurs to an appreciable extent, a limit on the velocity therefore limits the useful thickness of the bed. $\Phi_2(L) - \Phi_2(0)$ can be assigned a maximum value based on data that might be taken on rotating-disk electrode. Equation 59 can then be solved for the velocity v. What is left to be specified, then, is the length of the electrode. The length of the electrode is governed by the desired degree of conversion. Equation 53 can be solved for L if y is replaced by αL and θ is replaced by θ_L, the desired conversion. In the case of neglecting the effect of axial dispersion and diffusion,

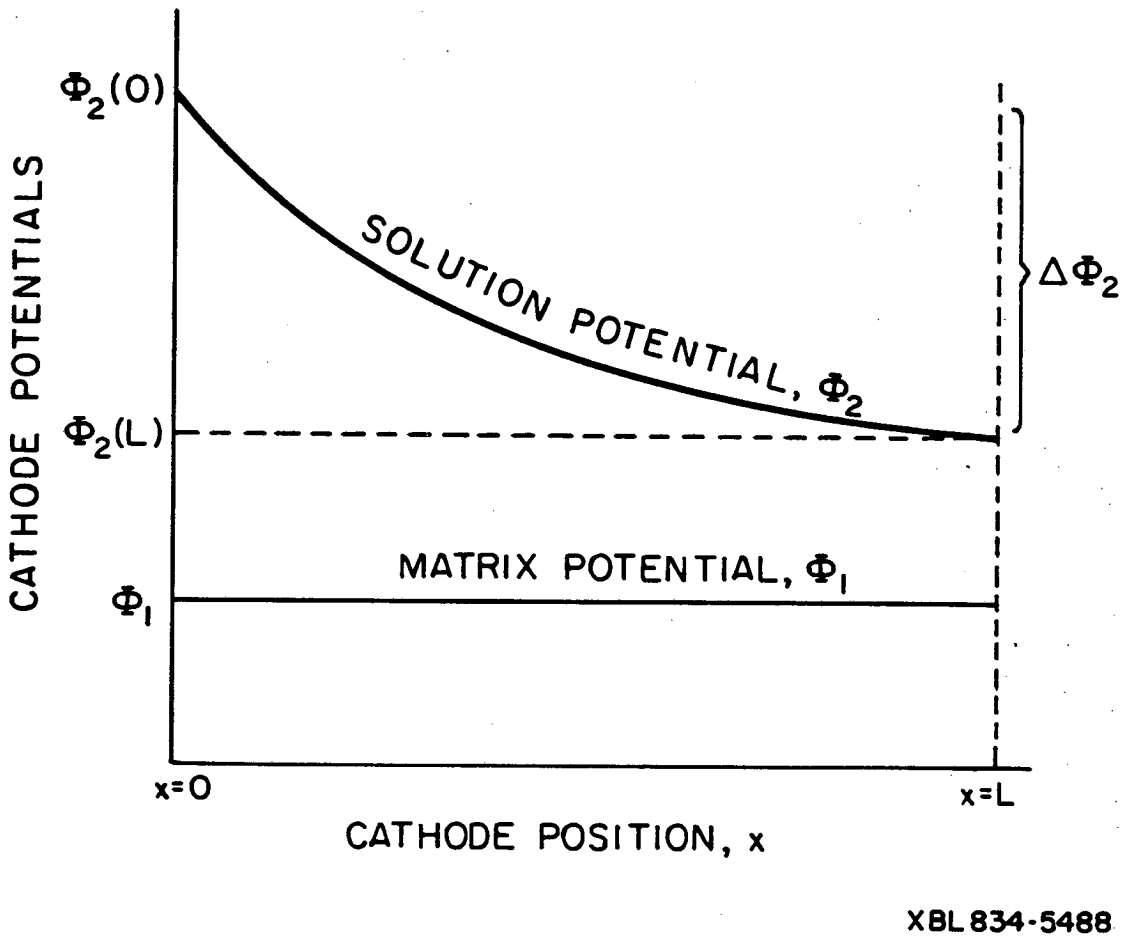

Figure 6. Variation of solution and matrix potentials as a function of position through a porous cathode. Matrix conductivity is infinite.

$$L = \frac{v}{ak_m} \ln \left(\frac{c_0}{c_L} \right). \tag{60}$$

As mentioned above, other configurations of anode placement and current collector placement can be considered.[53] Qualitatively, an upstream counterelectrode will yield the highest reactant concentration and the highest potential driving force at the front of the electrode. A downstream counterelectrode will have the maximum reactant concentration where the potential driving force is smallest. Thus this latter configuration might appear to give a more uniform reaction distribution throughout the bed. It is important then to consider the best configuration to achieve a given objective. Calculations show that the best configuration for achieving low effluent concentrations is with an upstream counterelectrode. This rule applies for both high or low ratios of σ/κ. In fact, a limiting current distribution cannot be achieved for a system utilizing a downstream counterelectrode (except for short reactors). For very high values of σ/κ, the matrix potential is constant, and placement of the current collector is not important. For moderate matrix conductivities the optimum placement of the current collector depends on the particular chemical system being investigated and the actual value of σ/κ.

We have considered above that often a flow-though porous electrode may be ohmically limited. This suggests an alternative configuration seen at the bottom of figure 7. The flow-by porous electrode configuration has the advantage that the flow of current is perpendicular to the fluid flow. The electrodes can be made thin to minimize the ohmic potential drop in the electrodes, and they can be made long to achieve high conversions. The disadvantage of the flow-by configuration is the necessity of including a separator to avoid anolyte and catholyte mixing. The mathematical analysis is also inherently more complicated due to the two-dimensional nature of the problem. Two dimensional modeling work has been done by Alkire and Ng.[54] They treat a cylindrical packed-bed electrode surrounded by a concentric counterelectrode. Trainham and Newman[55] present an engineering model that compares the performance on an economic basis of the two porous electrode configurations for redox energy storage. The results of the computer optimization show that the flow-by configuration is superior in this case, where the dimensionless quantity $\epsilon nFD_o c_o / s_R \kappa \Delta\Phi_2$ is large. For dilute solutions (small values of $\epsilon nFD_o c_o / s_R \kappa \Delta\Phi_2$) the flow-through configuration may

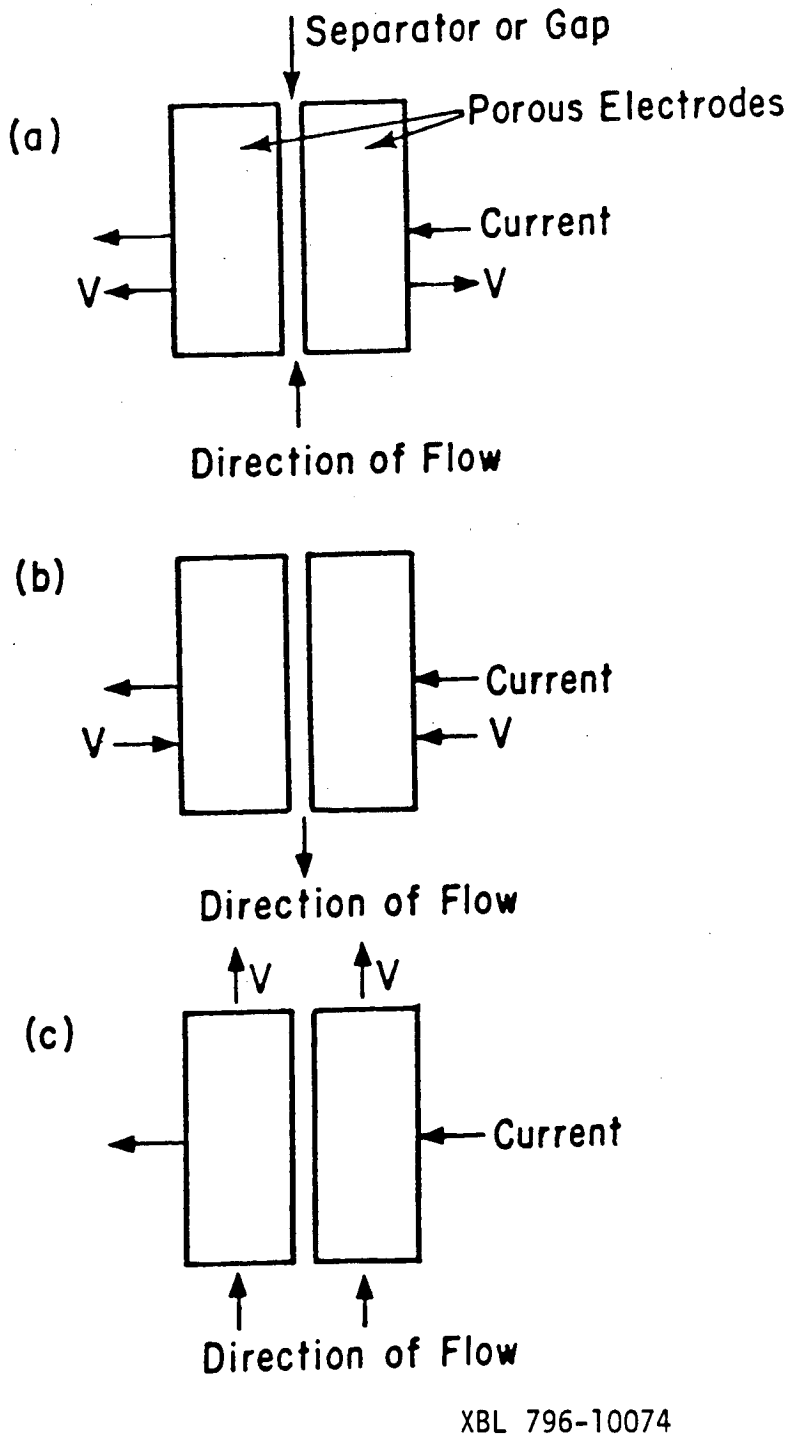

Figure 7. Various configurations of electrode placement relative to the direction of fluid flow. (a) and (b) are flow-through configurations (current and fluid flow are parallel), and (c) is the flow-by configuration (current flows perpendicular to fluid flow).

continue to have merit. Fedkiw[56] presents a comparison of the performance of flow-through and flow-by electrodes operated at limiting current. For a given maximum ohmic potential drop and desired conversion, he concludes that a flow-by electrode with a length to width aspect ratio greater than 5 will have a higher processing rate than a flow-through electrode. An ultimate design of a flow-by electrode must recognize that it can be run below the limiting current.

It is clear that the flow-by system holds sufficient promise that more detailed mathematical modeling and scale-up criteria are needed. The zinc-bromine secondary battery system as well as flow-redox energy storage systems have evolved to flow-by configurations.

3. Battery Applications

Let us now focus attention on the use of porous electrodes for battery applications. Several levels of mathematical sophistication can be used to examine battery systems. Initially we should like to develop guidelines for screening prospective systems. As development of a new or old system continues, we then resort to more sophisticated mathematical models for our design and scale-up. Before going into details, let us consider some general aspects of battery systems.[57]

We wish to examine desirable characteristics for batteries so that we may define inherent limitations or areas needing development for new and existing systems. One recognizes that listing a set of desirable characteristics implies a particular application. In examing a new or old system we wish to look at advantages and disadvantages in terms of cost (perhaps amortized cost/cycle), energy and power density, shelf life, reversibility, energy and coulombic efficiencies, material utilization efficiency, cycle life, reliability, portability, safety, and availability of materials.

One of the first characteristics of a battery to be considered is its voltage and specific energy. Knowledge of the overall reaction allows calculation of the open-circuit potential from thermodynamic data. Dividing the potential by the equivalent weight (kg/C) yields the theoretical specific energy of the electrode pair. Thus, more energetic electrode couples with lower equivalent weight will increase the theoretical specific energy. From a practical viewpoint, the advantage of more energetic couples must be weighed against the more severe materials compatibility requirements in the more corrosive environment. For new batteries the specific energy quoted is often a theoretical

energy based only on the mass of active materials. The theoretical specific energy of the lead-acid battery is 218 W-h/kg based on the active materials PbO_2, Pb, and H_2SO_4. Including the weight of the solvent (for an initial concentration of 5 M H_2SO_4) decreases the energy to approximately 100 W-h/kg. Addition of the weights of current collectors, excess active materials, separator, container, and connecting posts decreases this value further to approximately 40 W-h/kg. A rule of thumb that the final specific energy is 25 to 30 percent of the theoretical specific energy has been found to be approximately true for several systems. This rule should be used with caution, but it does illustrate the performance penalities associated with battery packaging and scale-up.

Knowledge of the specific energy of the system can be used to assess the promise of a given system. Data on the specific power of the system are also needed to determine the ability of the battery to deliver energy at different rates. The maximum specific power that a battery can deliver can be approximately calculated by $(U/2)^2/R_i$ where U is the open-circuit potential and R_i is the sum of the internal area specific resistances (Ω-cm^2) times the loading density of material (kg/cm^2). The area specific resistance can be estimated on the basis of electrolyte conductivity and separator thickness. Battery designs with large current densities should keep overall area specific resistances down to approximately to 1 Ω-cm^2 and keep area specific resistances of the separator itself down to about 0.2 Ω-cm^2. These calculations become more refined as we obtain more information on a system. Higher specific energies and specific powers are important in applications where total weight or volume are important. In electric vehicle applications, for example, a battery may not have enough energy or power to carry itself and its support structure.

Three system efficiencies characterize the performance of a battery. Coulombic efficiency is a measure of the reversibility of the electrodes or the presence of side reactions. Is is given by the ratio of the number of coulombs released during discharge to the number of coulombs required to charge the system back to its initial state. Energy efficiency is calculated by multiplying the coulombic efficiency by the ratio of average discharge voltage to average charging voltage. Differences in charge and discharge voltages are due to irreversibilities associated with the ohmic potential drop in the solution and matrix, and overpotentials associated with electrode kinetics and mass-transfer resistances. Coulombic efficiencies can often approach 100 percent, while energy

efficiencies are typically 50 to 80 percent. The method of charging and discharging the battery will affect both of these numbers.

The material utilization efficiency is the ratio of the actual coulombs passed during discharge to the theoretical amount of active material available. Utilizations of 70-80 percent are typical, and again are dependent on the method of discharge as well as any imposed cut-off voltage. Material utilizations often decrease with cycling. Among the factors that can lead to material utilizations less than 100 percent are the isolation of active materials, solubility problems with reactants and products, and, as mentioned above, any imposed voltage cut-off. Isolation of active material can occur when an insoluble, insulating reaction product covers the active material. Highly nonuniform reaction distributions can lead to pore blockage. Differences in the molar volume of reactants and products cause porosity changes which can lead to matrix fracture.

The solubility of reactants and products is important to material utilization as well as cycle life and shelf life. Dunning[58] identifies a range of approximately 5×10^{-5} to 11.4×10^{-5} molar for the desirable solubility range of a sparingly soluble reactant. The lower limit of solubility is based on the need to diffuse the reactant to the active sites from sparingly soluble crystallites. The ability to store the reactant in close proximity to the active site was listed as one of the advantages of porous electrodes. The upper limit of solubility can determine the shelf life of the cell because of self-discharge processes. In general, a soluble reactant on discharge will react if it can diffuse to the other electrode, while a soluble reactant on charge will be substantially inert if it diffuses to the other electrode. A soluble discharge reactant can be permanently incorporated into the other electrode and not be recoverable on charge. The magnitude of solubility also influences the redistribution of active material. The relatively high solubility of ZnO in KOH leads to marked concentration changes on cycling, and these can couple with the fluid flow to produce zinc shape change.[59,60]

We have mentioned above that the method of charging can affect the efficiencies of a given system. Ideally the charging process will restore the battery to its state at the onset of the discharge cycle. In general the charging process plays an important role in the cycle life and performance of a battery. Two common charging methods that may be used are constant current and constant voltage.

These can be combined with voltage or current limits to help minimize side reactions, or for thermal management. Side reactions, however, often do occur on charge. If these reactions occur preferentially on one electrode, an imbalance in state-of-charge occurs. The ability of the system to accept overcharge then becomes important. More sophisticated charging procedures can be developed, but may be prohibitively expensive depending on specific applications. In some redox energy storage systems, for example, a third electrode is used to correct for imbalances in state-of-charge.

Porous battery electrodes can be constructed in a variety of configurations. Often individual electrodes are constructed with a highly conducting, inert substrate (grid) that mechanically holds the porous matrix in place. It should be strong enough to withstand volume changes on cycling and be inert over the operating temperature and voltage ranges. For a battery plate with poorly conducting active materials, the grid is necessary to act as a current collector to conduct electrons to or from the reaction site. For moderately conducting active materials it can act as a secondary current collector. In electrode configurations using grids, the current is collected from each plate and is connected in parallel with an interconnecting bus. The optimal design of the current collecting grid and intercell connectors is a scale-up problem that will be considered later. Another battery configuration that can be considered is a bipolar arrangement. Such an arrangement eliminates the need for a separate current collecting grid for each electrode and may possibly minimize the voltage and weight performance penalties associated with the grid. Here the positive and negative active materials are put on opposite sides of an inert, conducting substrate. Current flows straight through the cell stack and is collected at the ends. The materials constraints for the conducting substrate are severe; it must be substantially inert to both the oxidizing and reducing environment. Corrosion of the substrate will lead to short circuits.

Materials compatibility is often a major problem in new or old battery systems. Materials constraints may limit cycle life or prohibitively increase the cost of a system. For example, corrosion of the current collecting grid is cited as a major failure mechanism for the lead-acid battery. Active material in ambient temperature Li electrodes becomes electronically isolated from its substrate, presumably due to reaction with impurities and the electrolyte itself.[61] In general we look for a battery system where the active materials are compatible with each other and the other support

materials required in the battery. We require the electrolyte, separator, battery container, interconnecting bus and post, current collectors, *etc.* to be stable over the operating voltage and temperature ranges of our system while not catalyzing side reactions or otherwise reacting adversely with the system.

A separator is a major component of the battery package. It is is required to separate the positive and negative electrodes in the battery, so that they may be in close proximity but not short together. A common failure mechanism in early battery development is shorting of the positive and negative electrodes by dendritic growth of material through the separator.[59,60] Separators must be electronic insulators, but have relatively high ionic conductivities. A separator with a high area specific resistance (Ω-cm^2) leads to a high ohmic potential drop with subsequent poor performance. Separators may also be required to have other desirable properties. Often they should be specifically conducting to only certain ionic species[59,60] or must contain additives that increase electrolyte wetting.

Costs, of course, must always be considered within a particular application. Besides the costs of raw materials, some other factors can be considered. Costs associated with safety, recycling (particularly if availability of materials is low), and associated environmental factors need to be considered. A common basis for comparison of various alternatives of secondary batteries is the amortized cost of the system in \$/W-h-cycle.

Scale-up of porous electrodes is not straightforward. Simply increasing the thickness of an electrode, for example, does not necessarily bring about proportional increases in performance. We wish to develop a micro-model of the porous-electrode system so that we can predict the effects of changing parameters such as electrode thicknesses on the behavior of the system. Having this information in hand then leads us to couple the micro-modeling to further scale-up considerations of plate area and lengths of intercell connectors.

In examining the micro-modeling of porous electrodes let us first consider the zero-time behavior[62] where concentrations are assumed to be uniform throughout the pore volume. Further let us ignore double-layer charging effects. Four dimensionless ratios govern the current distribution.

These can be stated as a dimensionless current density

$$\delta = \frac{\alpha_a FIL}{RT}\left(\frac{1}{\kappa} + \frac{1}{\sigma}\right), \tag{61}$$

a dimensionless exchange current

$$\nu^2 = (\alpha_a + \alpha_c)\frac{Fai_0L^2}{RT}\left(\frac{1}{\kappa} + \frac{1}{\sigma}\right), \tag{62}$$

the ratio of transfer coefficients in the polarization equation α_a/α_c, and the ratio of effective solution and matrix conductivities κ/σ. δ and ν^2 are ratios describing the competing effects of ohmic potential drop and slow electrode kinetics. For large values of δ or ν^2, the ohmic effect dominates with a nonuniform reaction distribution. For small values of κ/σ, the reaction occurs preferentially near the electrode-separator boundary at the expense of the region near the backing plate.

The nonuniformity of the reaction distribution for Tafel kinetics can be seen in figure 8. For Tafel kinetics the current distribution depends only on the parameter δ and the ratio κ/σ. Curves for linear polarization would exhibit similar behavior as in figure 8. For linear behavior, the distribution becomes nonuniform for large ν and is independent of the total current. For both cases, the ratio of κ/σ serves to shift the reaction distribution from one face to the other.

The distance to which the reaction can penetrate the electrode determines how thick an electrode can be utilized. This penetration depth is characterized by

$$\frac{L}{\nu} = \left(\frac{RT\kappa\sigma}{(\alpha_a + \alpha_c)ai_0F(\kappa + \sigma)}\right)^{1/2}. \tag{63}$$

Electrodes much thinner than the penetration depth behave like plane electrodes with an enhanced surface area. Electrodes much thicker are not fully utilized. For high current levels, in the Tafel range, the ratio L/δ will be more characteristic of the penetration of the reaction.

To continue to follow the discharge behavior of a porous electrode through the transient behavior, we need to consider the time derivative in equation 33. Porous electrodes used in primary and secondary batteries invariably involve solid reactants and products, and the matrix is changed during discharge. Consequently, no steady state is strictly possible. We may nonetheless examine a

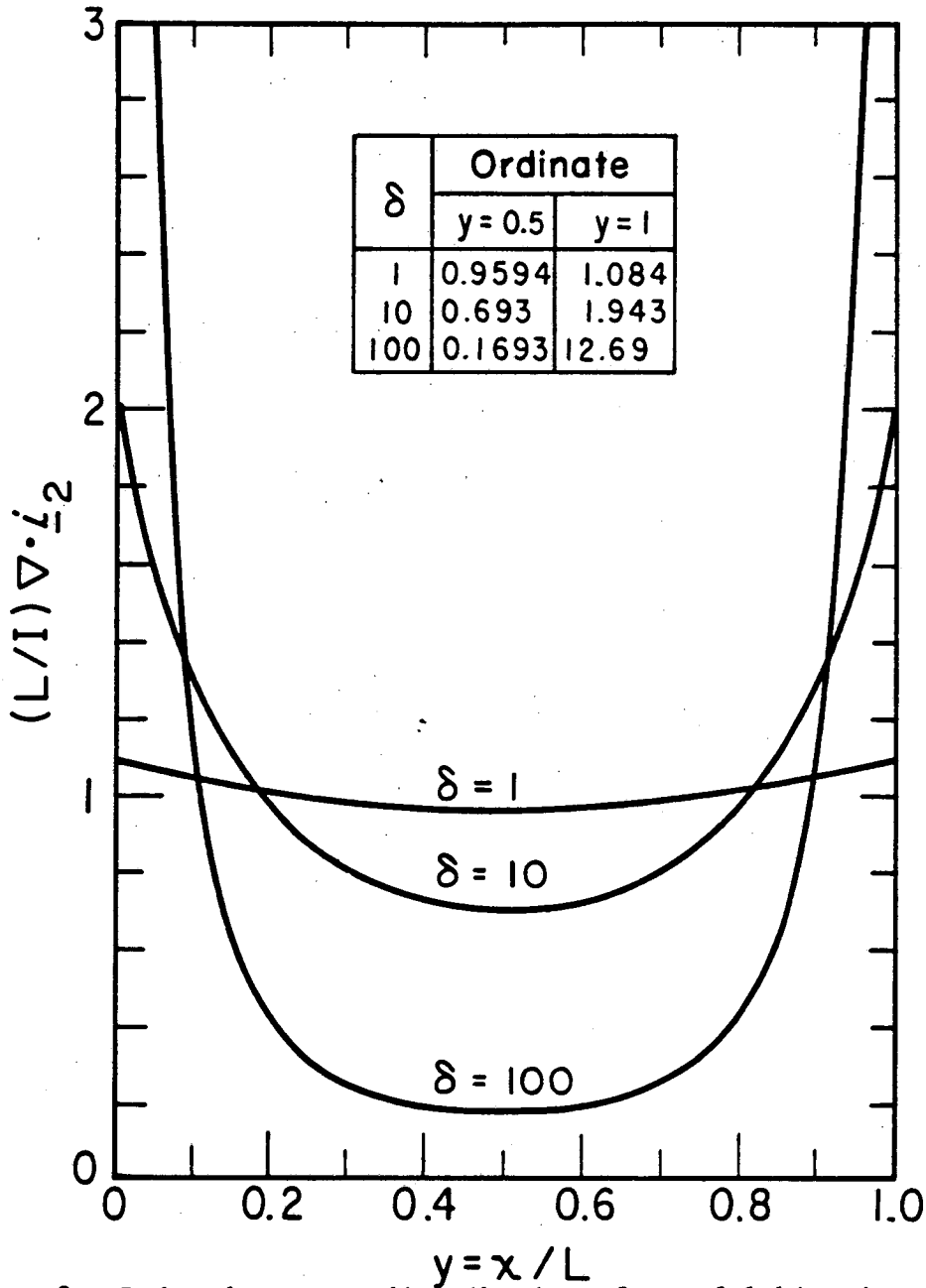

δ	Ordinate	
	y = 0.5	y = 1
1	0.9594	1.084
10	0.693	1.943
100	0.1693	12.69

Figure 8. Reduced current distributions for Tafel kinetics with equal matrix and solution conductivities.

XBL748-3782

steady-state operation of a porous electrode. Just above we have considered the irreversibilities associated with electrode kinetics and ohmic potential drop. As the reaction proceeds, reactant is depleted at the pore-solution interface. This then represents an additional irreversibility. Newman and Tobias[62] also treat a redox reaction in a porous electrode. Convection is assumed to be absent, and migration is neglected due to an excess of supporting electrolyte. The stoichiometric coefficients of the reactant and product species are taken to be +1 and −1. For a redox reaction equation 41 is often written as

$$\nabla \cdot \mathbf{i}_2 = a i_0 \left\{ \frac{c_1}{c_1^0} \exp\left[\frac{\alpha_a F}{RT} (\Phi_1 - \Phi_2) \right] - \frac{c_2}{c_2^0} \exp\left[\frac{-\alpha_c F}{RT} (\Phi_1 - \Phi_2) \right] \right\}. \tag{64}$$

Now i_0 is a constant representing the exchange current density at the composition c_1^0, c_2^0. The potential difference $\Phi_1 - \Phi_2$ is equal to η_s plus an additive term which depends on the local solution composition. (Compare this with equations 10 and 11.) A new dimensionless group $\gamma_i = s_i IL / nF\epsilon D_i c_i^0$ can be formed due to the introduction of the diffusion coefficient of each species and a characteristic concentration. Another special case that can be treated is deposition from a binary electrolyte. The binary electrolyte formulation can be applied to sulfuric acid in lead-acid batteries or to the polysulfide in the sodium-sulfur cell if the melt is taken to be composed of Na_2S and S. This formulation also applies to systems with concentrated KOH electrolyte such as in Ni-Fe and Ni-Zn cells, although the solubility of ZnO must be ignored.

Often a system cannot be approximated by one of the limiting cases presented above. Full treatment of the complicated factors governing the behavior of the porous electrode requires the use of high-speed digital computation. Newman and Tiedemann[36] suggest a computational method for battery electrodes involving a binary electrolyte. In general reactant species are depleted during the course of discharge, and time must be included as a variable. Thus the coupled equations are solved simultaneously at each time step. Pollard and Newman[63] treat the transient behavior of the lithium-aluminum, iron sulfide high-temperature battery for a constant current discharge. Concentration distributions across the cell sandwich are presented at various times throughout the discharge.

In summary we can list a number of factors which can affect the performance of porous electrodes:

1. Charge and discharge methods affect battery efficiencies and cycle life.
2. The solubility of reactants and products can limit cycle life and shelf life.
3. Higher current densities yield higher overpotentials, and thus a given cutoff potential is reached sooner.
4. The pores may become constricted or even plugged with solid reaction products. A nonuniform reaction distribution will accentuate this problem at the mouth of the pores.
5. Utilization of the solid fuel can be limited by covering of the reaction surface with reaction products.
6. Rates of mass transfer between crystallites and the reaction surface may become more limiting as the discharge exhausts the front part of the electrode. This could account for changes in the apparent limit of utilization with current density.

Until now we have considered the mathematical modeling of porous battery electrodes. Experimental data are needed, of course, to insure that our understanding of the system is substantially correct. In constructing an experimental cell we want to eliminate any scale-up effects not included in the mathematical modeling so that we can directly compare experimental and theoretical results. The scale-up effects of current collectors and interconnecting bus and post will then be considered separately.

The experimental system can be arranged in a mono-cell configuration with one positive and one negative plate, or as a bi-cell with a single positive electrode and two negative electrodes. The bi-cell arrangement represents a "section" of a positive and two half negatives that would be found in the scaled-up battery. The construction and symmetry of discharge of this cell would be similar to the scaled-up version. The mono-cell's main advantage over the bi-cell may be in the ease and cost of construction.

A schematic of the bi-cell is shown in figure 9. This figure shows heavy, highly conducting current collecting sheets in the center of the positive electrode and at the back of the two half nega-

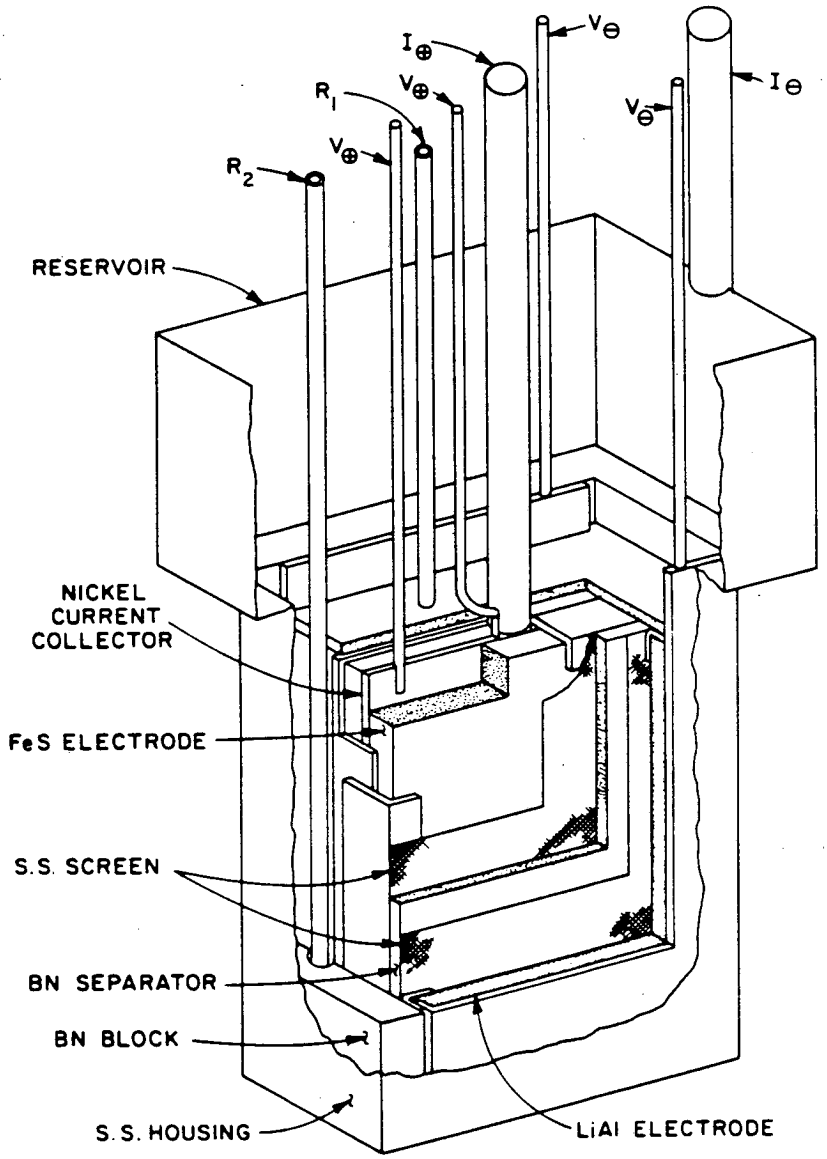

XBL 834-9115

Figure 9. Bi-cell design of a positive and two half negative electrodes designed to promote a uniform current distribution across the electrode face.

tive electrodes. These current collectors promote a uniform current distribution across the face of the electrode by minimizing the ohmic potential drop in the current collecting sheet. This is important for comparison to one-dimensional micro-modeling results or for use as data in subsequent scale-up calculations. Separate voltage and current taps should be used to eliminate any error in voltage readings due to ohmic potential drop in the cell leads. Reference electrodes should be used in the experimental cell so that the total cell potential can be decomposed into contributions associated with the positive and negative electrodes. Although we will see that this decomposition is not necessary for our scale-up calculations, research efforts at improving the battery need to be largely directed to the limiting electrode. Batteries are often designed so that the positive electrode limits the battery capacity. This should then be the case with the experimental cell as well. In general it is important to use the same electrode thicknesses, amount of active material, excess electrolyte, temperature, separator material, *etc.* that is being considered for the scaled-up version. Micro-modeling results can be used a a guide in the selection of some of these parameters. The cross-sectional area of the test cell is not important since our experiment is designed to be one dimensional.

The current is measured during discharging or charging with a current-interruption technique. The cell potential during current flow ($\Phi_p - \Phi_n$) and after 15 seconds† of interruption is interpreted according to the equation

$$i = Y(U - \Phi_p + \Phi_n) , \tag{65}$$

where i is the current density from negative to positive plate (A/cm^2), Y is the conductance of a cell element (Ω^{-1}-cm^{-2}), U is the apparent open-circuit potential (V), Φ_p is the potential of the positive plate (V), and Φ_n is the potential of the negative plate (V). This relationship assumes a linear polarization curve; however it can also be regarded as a step in the linearization of a non-linear problem. Values of U and Y can be determined as a function of the state of charge for a given con-

†When the total external current is interrupted, we can identify three transients: relaxation of the double-layer capacity, a local equalization of charge and concentration from front to back of the electrode, and a reduction of concentration gradients in the whole cell by diffusion across the separator. In the current-interruption technique, we wish to wait long enough for double-layer charging to relax. A characteristic time for this is L^2aC/κ. The apparent open-circuit potential will continue to rise as the other transients continue. We choose 15 seconds here so that we may more closely approximate the results that would be obtained with a 15-second power test.

stant current density. Data for a lithium-aluminum, iron sulfide high temperature cell taken at Argonne National Laboratory[64] are given in figure 10. The use of reference electrodes allows the decomposition of the cell potential and specific conductance into values for the individual electrodes. These values are related to the cell values by

$$U = U_+ - U_- \tag{66}$$

and

$$\frac{1}{Y} = \frac{1}{Y_+} + \frac{1}{Y_-}. \tag{67}$$

These results form a basis both for comparison to micro-modeling results and now for scaling up the plate size.

Cost, weight, and volume considerations dictate that the current collectors will not be the heavy plates used in our test cell. The mass of the current collector that should be used for a given plate area is a scale-up consideration that is subject to optimization. Our goal is to develop a discharge curve for the plate as a whole (with current collectors) based on individual cell elements shown in figure 10. Two common configurations for the current collector is the sheet current collector and a grid current collector. Tiedemann and Newman treat the nonuniform current and potential distributions in composite sheet electrodes[65] and in battery plates with grid configurations.[66]

The lead-acid battery uses a current collecting grid with the active material pressed between the ribs. A honeycomb grid has been used in experiments with the lithium-aluminum, iron sulfide battery. We choose as an operational current-collector model a rectilinear grid with horizontal and vertical elements. A one-dimensional micro-model[67] or data as in figure 10 is coupled to a two-dimensional model of the grid. Equation 65 can still be used where the current, area, and potentials are now local values for node points on the grid. The polarization parameters, U and Y, are curve fit as functions of depth of discharge and local current density. Kirchoff's law is used with equation 65 to solve for the local potential distribution across the face of the plate during discharge.

Results of this analysis give the overall plate behavior as a function of state of charge. The current distribution across the face of the electrode is nonuniform at the beginning of discharge and

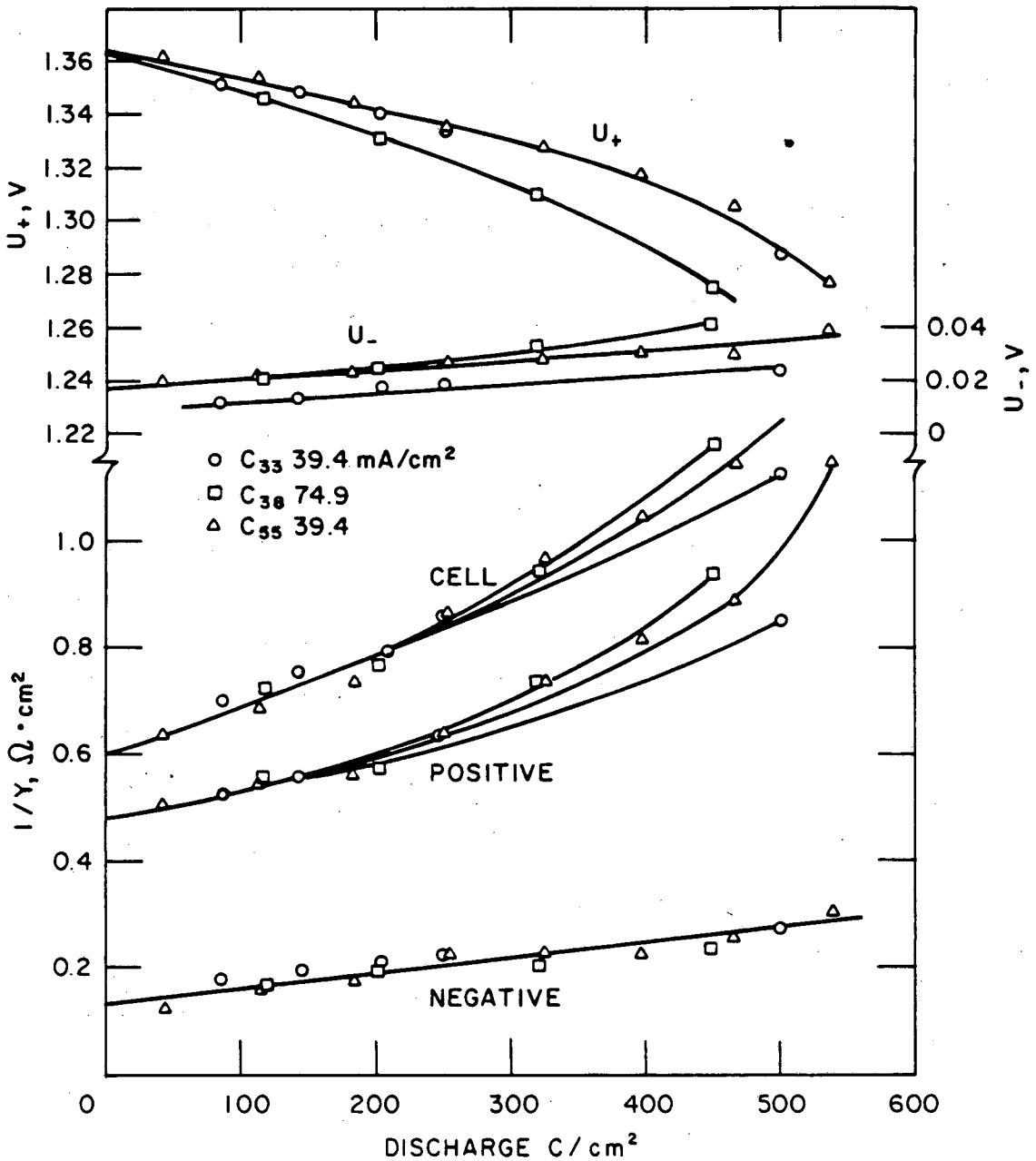

XBL 834-9116

Figure 10. Electrochemical characteristics (U and Y) on discharge for L_p = 0.32 cm and 30 percent excess capacity in the negative electrode.

becomes more nearly uniform as discharge proceeds because of the dependence of the electrochemical resistance and apparent open-circuit potential on the state of charge. The overall behavior can now be represented by

$$U - V = \Delta V = (R_g + \frac{1}{Y})i \ , \tag{68}$$

where ΔV is the voltage displacement from open circuit, and R_g is the resistance of the grid. Since $1/Y$ and R_g vary through discharge in ways that depend on the specific system, a general formulation of results cannot be made. However, we can consider the zero-time behavior of a system with constant polarization parameters and formulate the problem. For the primary variables ΔV the voltage displacement from open circuit, I the total current leaving the grid, A the area of the plate, Y the conductance of the cell element, M the mass of the grid, σ the grid conductivity, ρ the grid density, and L_p the positive electrode thickness, four dimensionless groups govern the system. One of these, L_p^2/A, does not have direct relevance to the problem. We are left with

$$\Pi_1 = \frac{I}{2AY\Delta V} \ , \ \Pi_2 = \frac{M\sigma}{\rho Y A^2} \ , \ \text{and} \ \Pi_3 = \frac{M}{\rho L_p A} \ .$$

Π_1 represents a ratio of overall conductance $I/2\Delta V$ to electrochemical conductance AY. Stated another way, Π_1 is the ratio of the actual current leaving the tab to the current that would leave the tab if there were no ohmic resistance in the grid. The factor of two in Π_1 reflects the fact that the total current leaving the grid tab is being collected from both sides of the plate. Π_2 represents a ratio of grid conductance $\frac{M\sigma}{\rho A}$ to electrochemical conductance AY. Π_3 is the volume fraction of grid material.

Other minor dimensionless parameters must now be chosen before the results of the grid model can be plotted. These include the ratio of the tab width to plate width, relative tab position, aspect ratio of plate height to plate width, ratio of total grid material on horizontal elements to that in vertical elements, and the number of horizontal and vertical elements, Further, results can be presented for an infinitely conducting negative grid, a symmetric negative grid with equal conductivity, or a complete description of a positive and negative with different conductivities.

Figure 11 is a plot of dimensionless plate current *vs.* dimensionless plate area for the beginning of discharge.[66] The volume fraction of grid material has been taken to be zero so that L_p does not enter as a parameter in this figure. Here the horizontal and vertical grid elements have the same amount of grid material, and a symmetric negative grid with equal conductivity is used. Figure 12 is an example of an improved grid. Extra conducting material has been added to the two columns of vertical elements below the tab and the horizontal elements across the top of the grid. The two center vertical elements are heavier by a factor of 11, and the top horizontal elements have 4 times the mass of the base elements. Figure 13 is a dimensionless graph of plate current *vs.* plate area for this grid design. Here the negative grid has been assumed to be infinitely conducting. A comparison of figures 11 and 13 shows the improvement in overall conductance for the improved grid design. This improvement is actually due to two major effects, the reduction of ohmic potential drop in the improved grid design and the neglect of ohmic potential drop in the negative grid.

Figure 14 is a dimensionless correlation of the same data as in figure 13. The dimensionless groups have been adjusted so that all the data closely follow the same curve. Here it is recognized that the grid necessarily displaces some active material, reducing the area for current within the bed. The active bed cross-sectional area is therefore $A - M/\rho L_p$. The area for current flow through the separator is A. Thus we correct the electrochemical conductance AY_0 by an additive contribution of separator resistance based on area A, and the rest of the electrochemical resistance based on area $A - M/\rho L_p$. Thus, $1/Y_0$ is replaced by

$$\frac{1}{Y_0}\left\{\frac{1 - Y_0 R_s}{1 - \dfrac{M}{\rho L_p A}} + Y_0 R_s\right\}$$

in plotting this figure. The value of the separator resistance, R_s (Ω^{-1}-cm^{-2}), can be estimated on the basis of electrolyte conductivity. The data plotted in this manner fall very closely on the same curve and have unity intercepts on both the ordinate and abscissa.

As pointed out above, figure 14 is strictly valid for zero-time behavior. Our alternative to performing complex grid calculations to map out the overall conductance during discharge is to assume

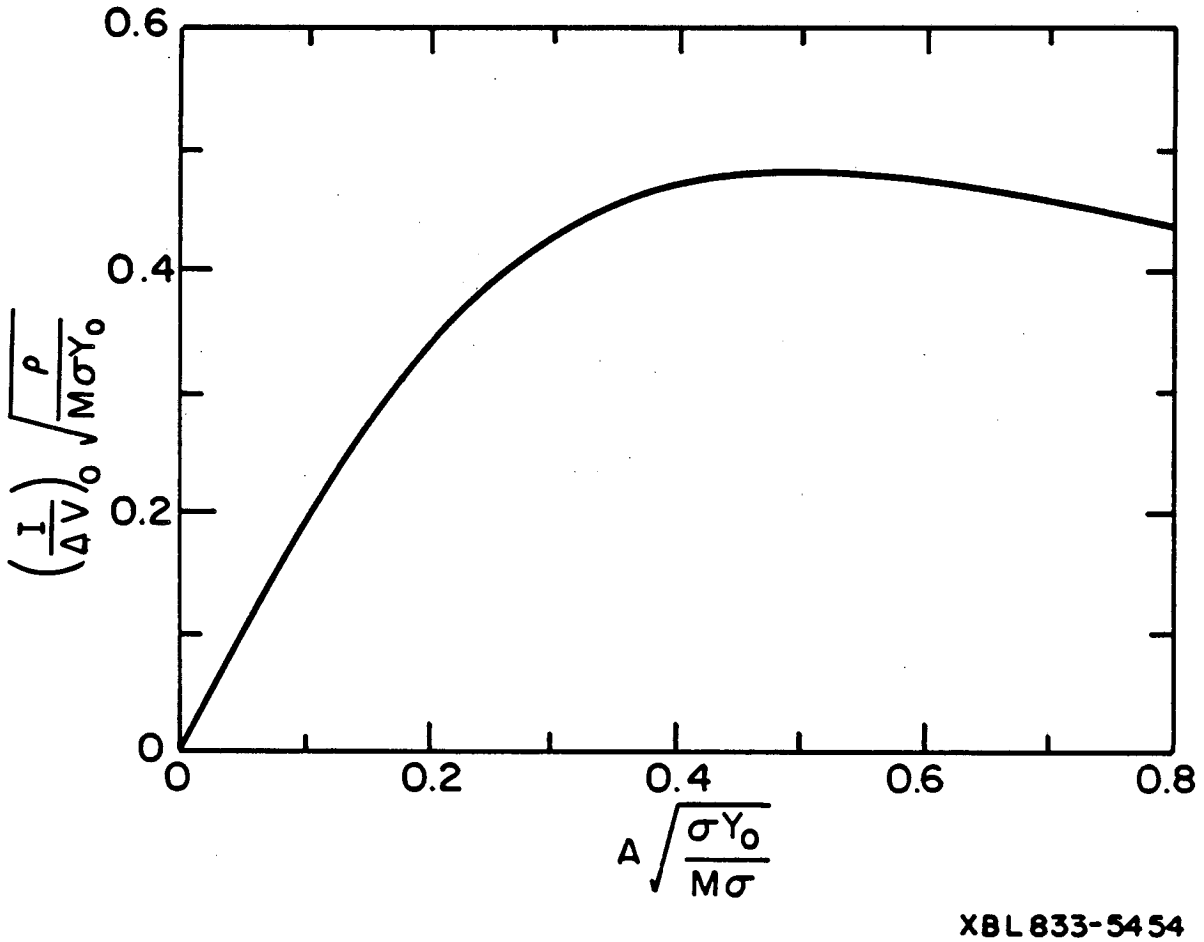

Figure 11. Dimensionless plate current as a function of the dimensionless plate area. Height to width ratio equals 0.8. Ten percent tab is located 30% from the edge of the place. L_p is taken to be ∞ . Reproduced from reference 66.

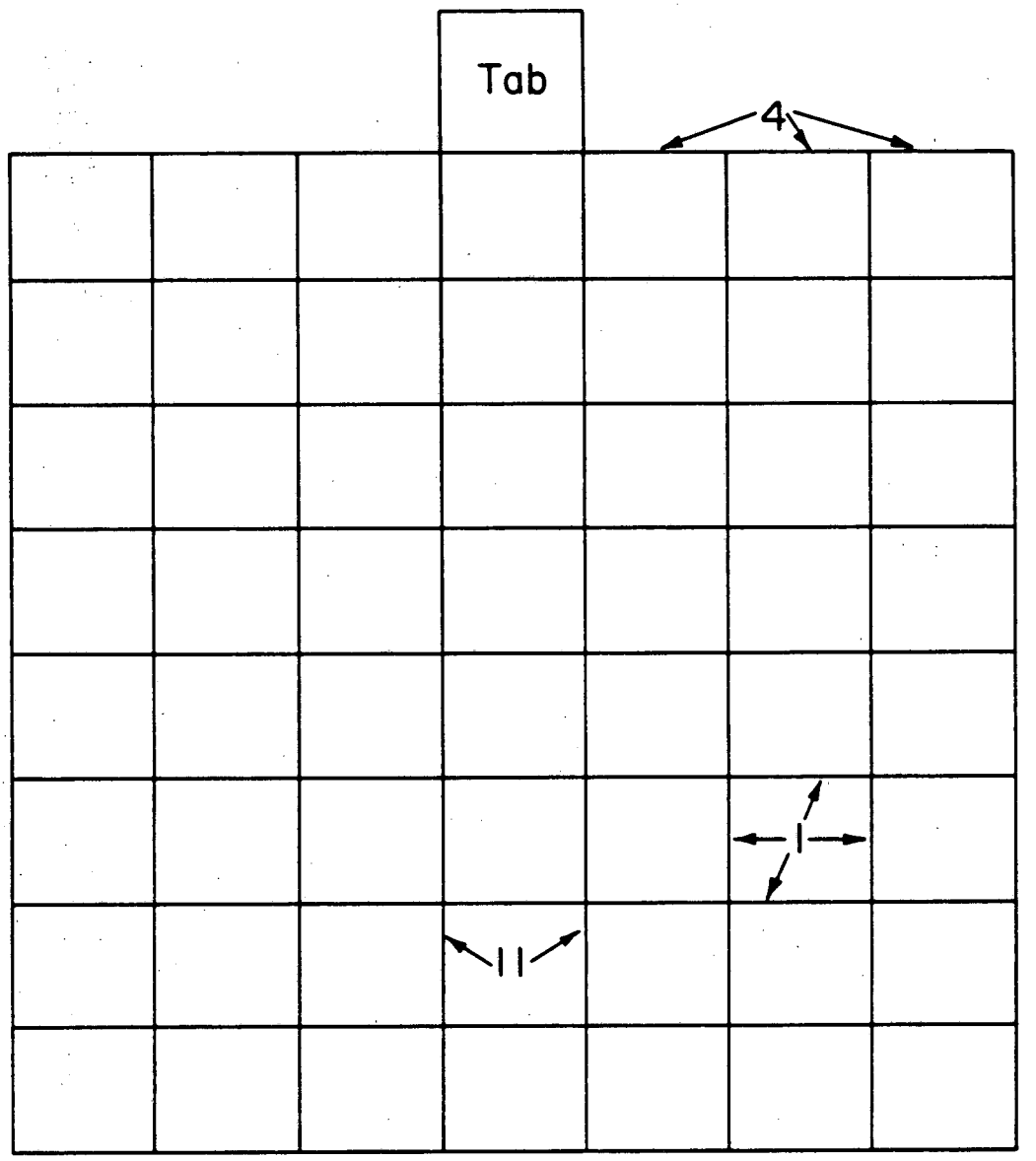

XBL 834-9114

Figure 12. Improved grid design with extra conducting material in the two vertical elements and top horizontal elements.

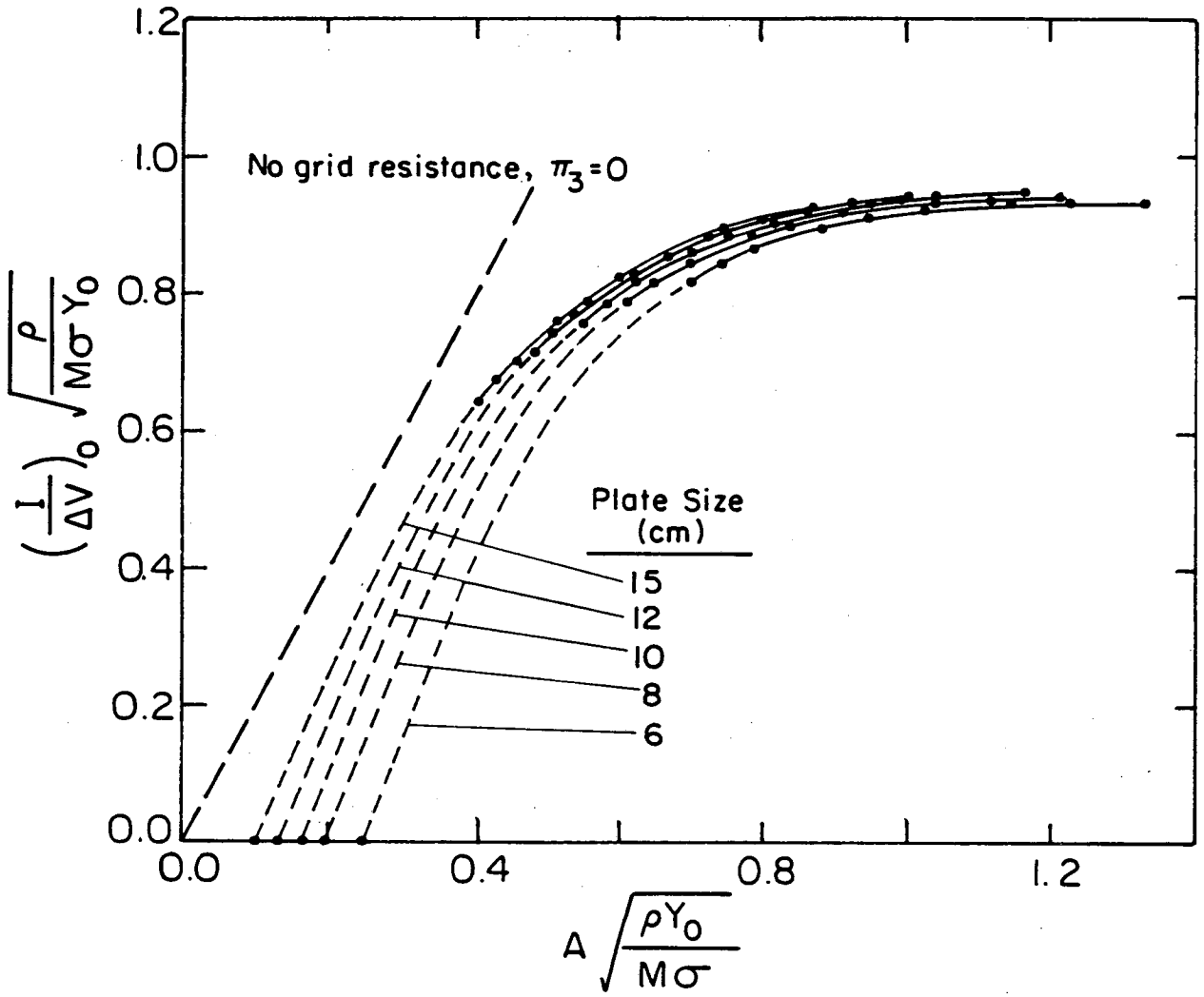

XBL833-5456

Figure 13. Dimensionless plate current as a function of the dimensionless plate area for the improved grid design.

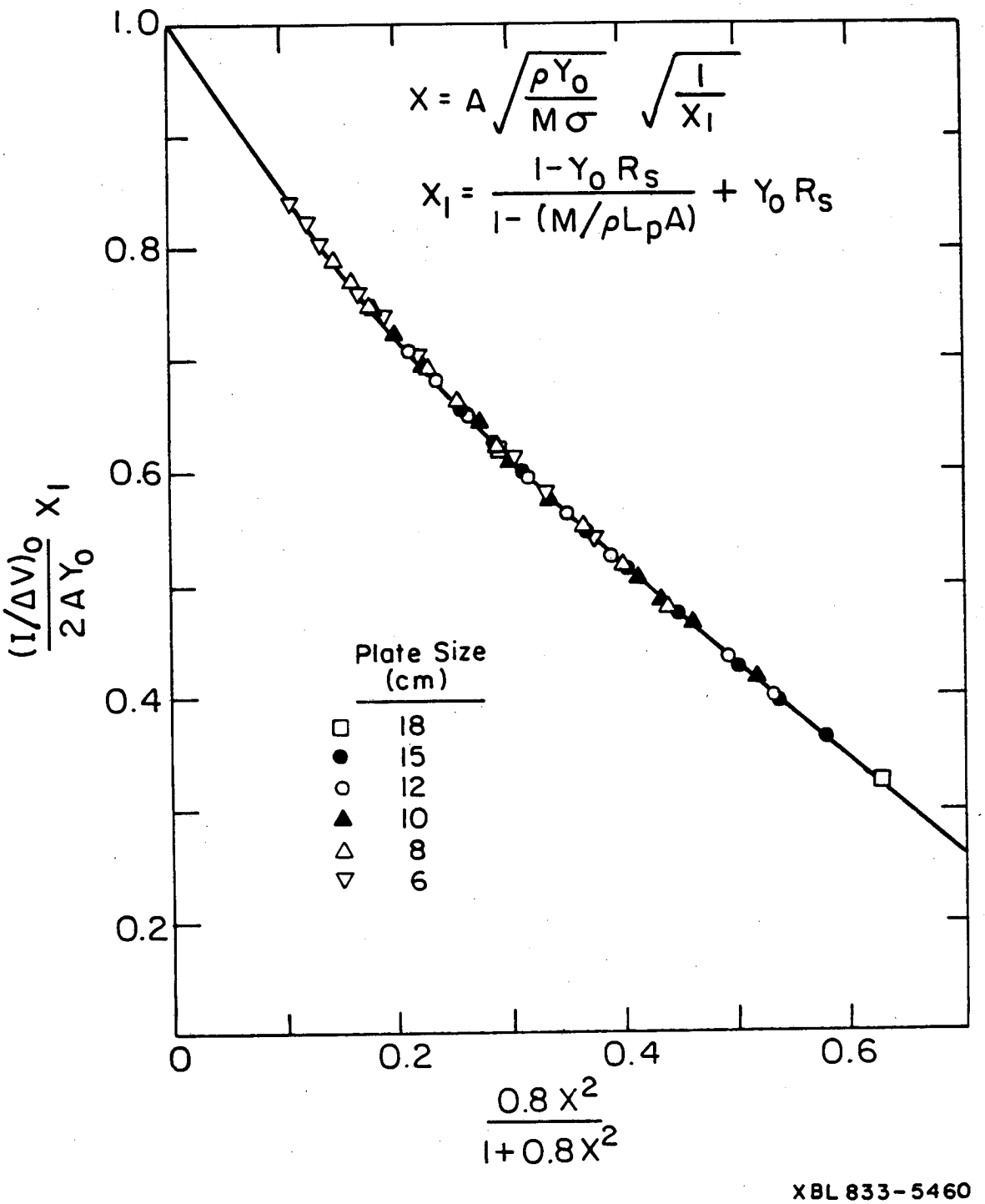

XBL 833-5460

Figure 14. Dimensionless plate conductance vs. dimensionless plate area based on a reduced area for current flow through the matrix bed.

figure 14 is valid throughout discharge, replacing Y_0 with Y and $(I/\Delta V)_0$ by $I/\Delta V$. Here we are recognizing the dependence of the polarization parameters on the average depth of discharge, but still assume that they are constant across the electrode face. Y and U actually depend on the local current density and local depth of discharge. This method should give a good approximation to the actual behavior of the plate and reduces to an exact solution to the complete grid formulation as the current densities become more uniform. A computer program can now be developed that uses data as in figures 10 and 14 to generate scale-up predictions for energy and power.

For a given plate size and grid weight, we can now calculate the specific energy and specific power through discharge. The calculations vary the average depth of discharge to a specified cut-off potential for a four-hour discharge rate. The results of these calculations, using the correlation in figure 14 and the data in figure 10, are given in figure 15. We immediately see a conflict in trying to optimize simultaneously the battery system for maximum energy and maximum power. Instead we choose an intermediate grid weight that gives a ratio of power to energy equal to the ratio of maximum power to maximum energy. Alternative compromises could be selected based on the particular applications at hand.

Having selected a natural system ratio for determining the grid compromise, we now recognize that our small cells must still be connected together in parallel with an interconnecting bus, and that the larger cell module must be connected in series to another cell module with an interconnecting post. Two important new parameters of the length of interconnecting bus and length of interconnecting post must now be considered. Figure 16 shows a symmetric arrangement of interconnecting buses for three positive electrodes. L_{bus} is approximately equal to the sum of the widths of the positive electrode, negative electrode, and two separators. The post represents the cell terminal plus intercell connector that extends from one cell module to the next cell module. In our calculations we take L_{post} to represent only that part of the post associated with one cell module, *ie.* the length of the terminal plus half of the length of intercell connector. The lengths of interconnecting buses for the positive and negative plates are taken to be the same, as are the post lengths. Given the post and bus lengths needed to connect our cells, an optimization of the distribution of conducting material among the parallel bus connections and the post connections can be made independently of other

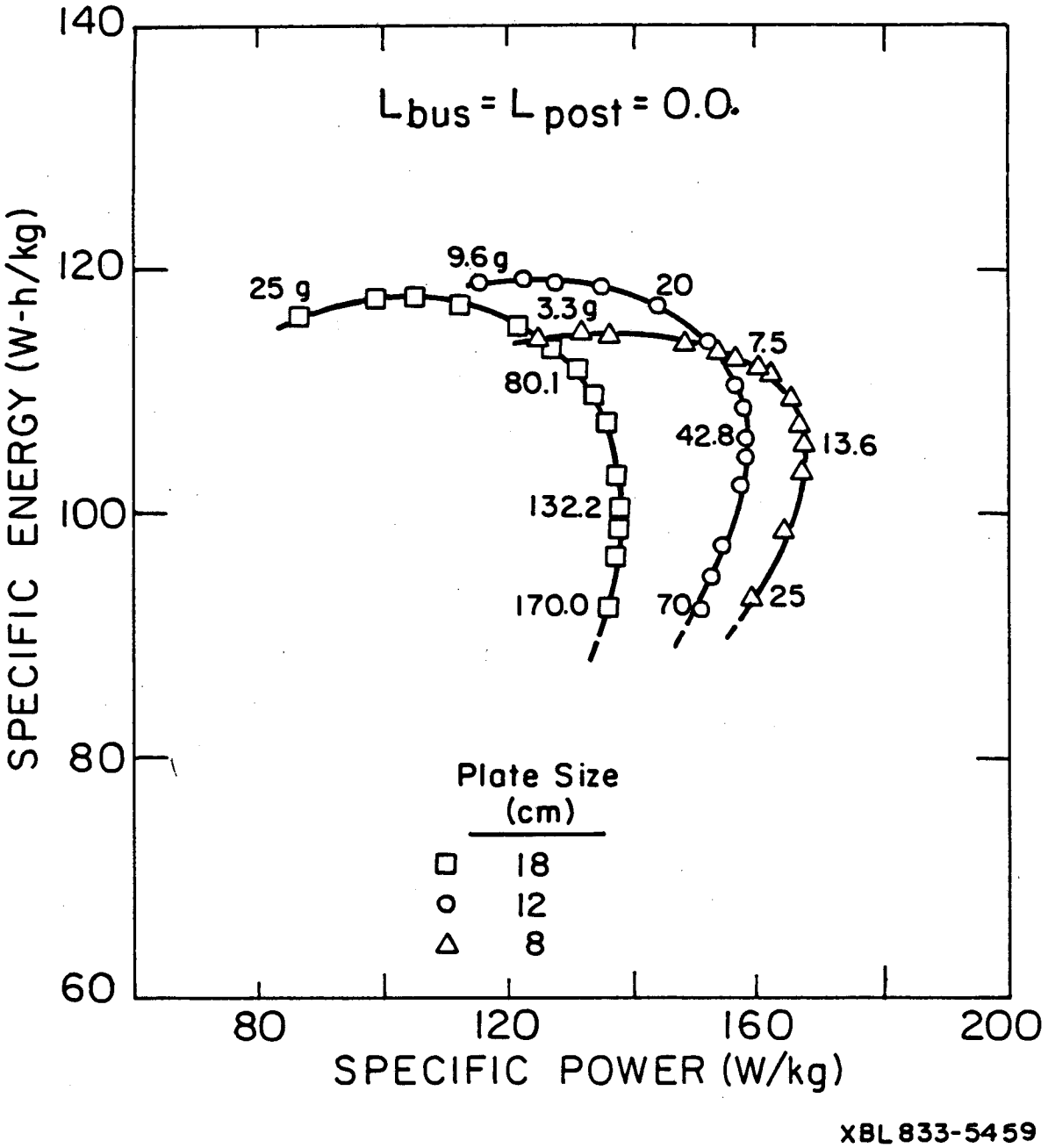

Figure 15. Maximum specific energy vs. maximum specific power halfway through discharge.

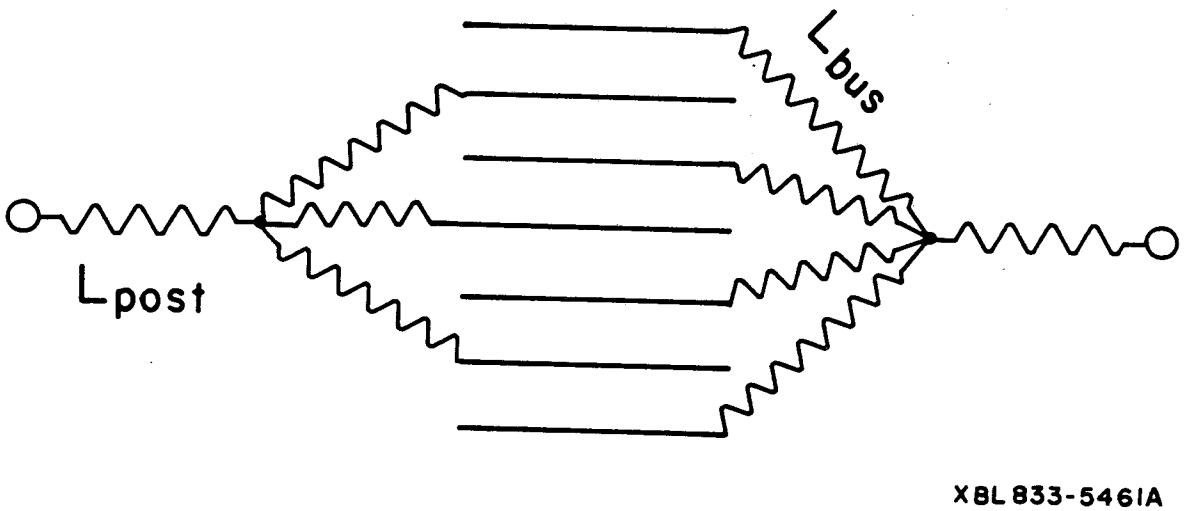

Figure 16. Symmetric arrangement of interconnecting buses and interconnecting posts for three positive electrodes.

scale-up considerations. The important quantity that results from this optimization is

$$L_{bus}\left(\frac{\rho_{bus}}{\sigma_{bus}}\right)^{1/2} + L_{post}\left(\frac{\rho_{post}}{\sigma_{post}}\right)^{1/2}.$$

If the density of the bus and post are taken to be equal, we see that only the sum of the bus and post length is important to the scale-up predictions. We also note that the number of positive electrodes per cell module is subject to variation. The number used will affect the final results for the power and energy, but does not affect the optimum distribution of material over the bus and post per cell "section."

For a given plate size and grid weight, the calculated specific energies *vs.* specific powers will form a loop in the same manner as in figure 15 as the mass of the bus and post is varied from very small values to larger values. Thus, for each plate area and grid weight we can find a mass of bus and post that maximizes either the specific energy or specific power. As we investigate different grid weights (and thus different optimum post and bus weights) we can find values of the mass of grid, bus, and post that yield the maximum power. Similarly we search for values of grid weights and bus and post weights that yield the maximum energy. Now our compromise ratio is the value of the maximum power to this maximum energy. Thus, for each plate size our compromise design is the values of the mass of grid, bus, and post that give a power to energy ratio equal to the compromise ratio. More than one combination of grid and bus and post weight will yield a power to energy ratio equal to the compromise value. The largest values of energy and power are selected from this collection of results to represent the best compromise design for a given plate area.

Figure 17 represents the composite prediction of specific energy *vs.* specific power as they relate to the size of plates and lengths of bus and post. Recall that each point given represents the best compromise of specific energy and specific power for each plate area as just discussed above. The performance penalty (weight and voltage) of including the interconnecting bus and post is readily seen. This graph can now be used to select the plate area which will give adequate performance at a suitable cost. The grid weights and plate areas used to generate figure 17 are plotted in figure 18. Also shown are the grid weights that correspond to maximum power and maximum

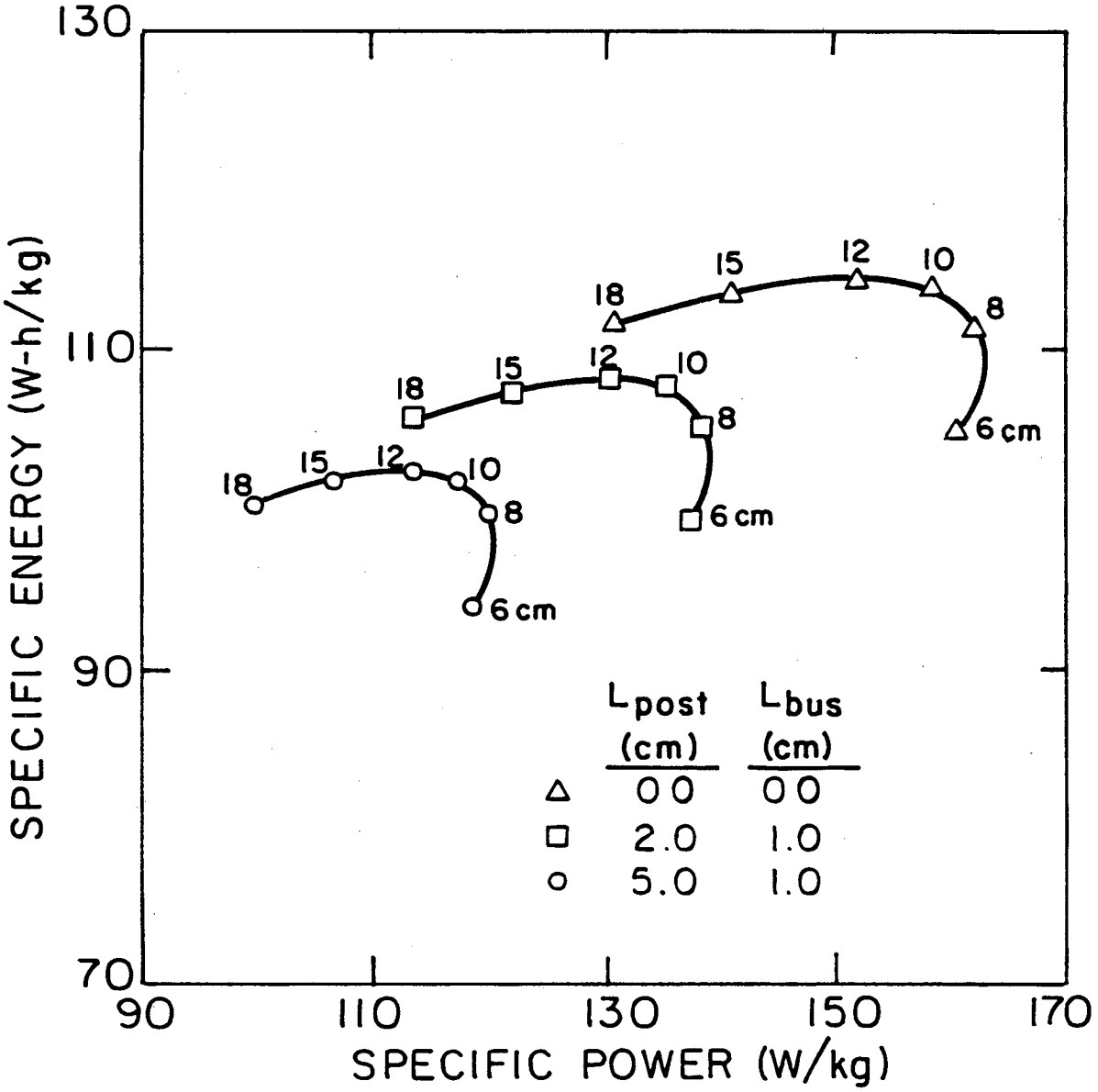

Figure 17. Composite, compromise predictions of the specific energy and specific power for various post and bus lengths and electrode areas.

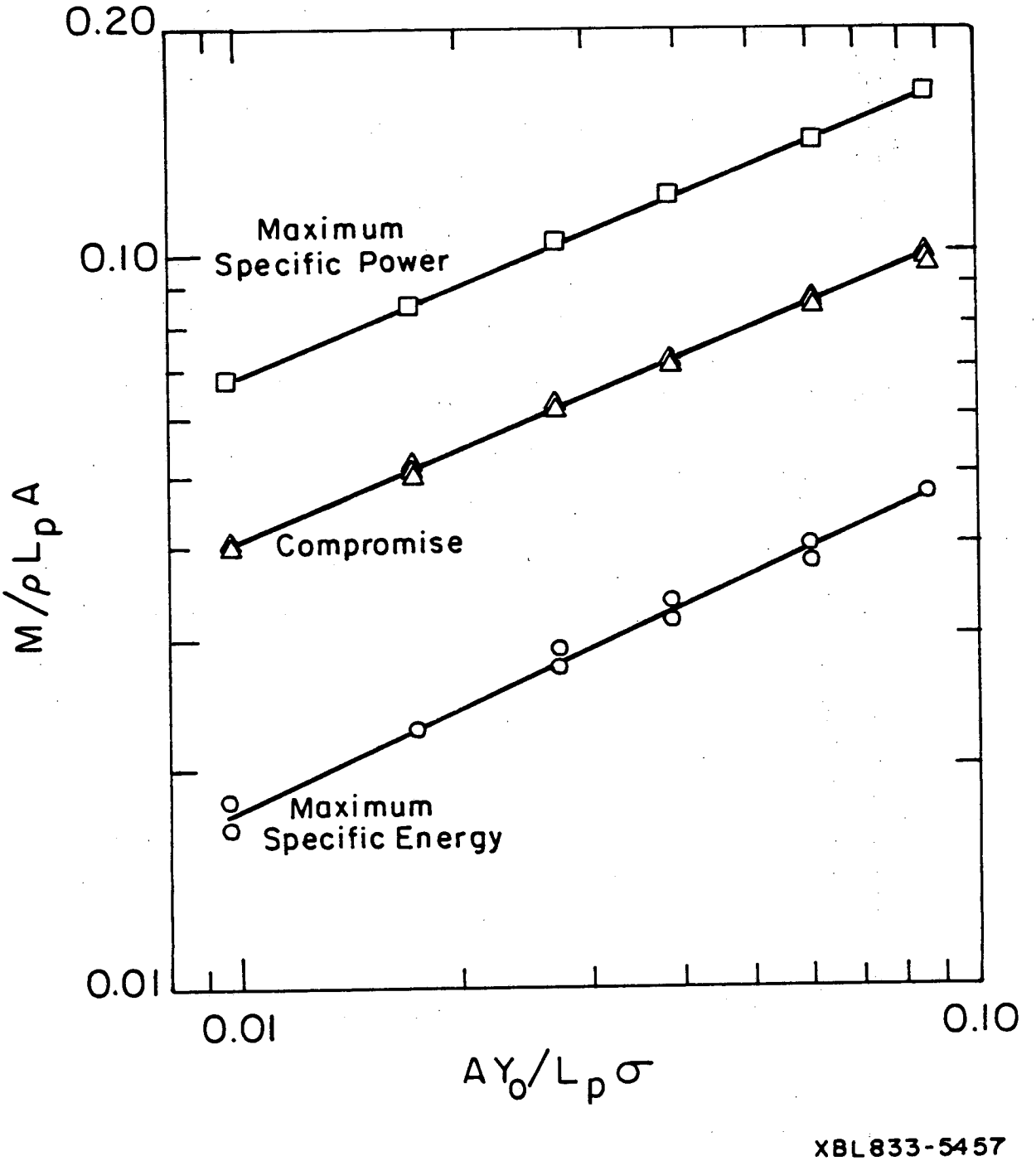

Figure 18. Dimensionless grid weight vs. dimensionless plate area along the maximum specific energy, maximum specific power, or the compromise design.

energy. This figure, then, yields the grid weight that gives the maximum power, maximum energy, or compromise for each plate area and length of bus and post. It is seen that the optimum grid weight is not greatly dependent on the length of the bus and post, and that this dependence is actually undetectable for maximum specific power. These results suggest that we can improve our grid design without concern over interaction with the optimum post and bus lengths, and that improvements may be independent of depth of discharge as well. We also see that the optimum grid weight should be roughly increased in proportion to $A^{3/2}$.

We should also note here that no consideration has been given to any minimum current-collector weight necessary to support the active materials through cycling. In general, for smaller cells it may be stated that a current collector that is large enough to contain the active material will have a weight large enough to approach or exceed the value corresponding to the design for maximum power. More detailed scale-up considerations are needed for bigger plate sizes. Finally we should note that the value of the grid weight corresponding to maximum specific energy will depend on the discharge time. As we decrease the discharge time from the four-hour value used here, the grid weight will move upward toward the value for maximum specific power.

In the results presented above, the delivered ampere-hour capacity of the battery has been a dependent variable. An alternative design sequence is to specify a value for the total delivered capacity. In this case the area of the plate is varied until the optimum values of grid weight and bus and post weight are found so that the specified capacity is reached at the cut-off voltage.

In summary we have shown how to account for the performance penalties associated with the grid and interconnecting bus and post.

ACKNOWLEDGMENT

This work was supported by the Assistant Secretary of Conservation and Renewable Energy, Office of Energy Systems Research, Energy Storage Division of the U. S. Department of Energy under Contract DE-AC03-76SF00098.

NOTATION

a	specific interfacial area per unit volume of porous electrode, cm^{-1}
A	cross-sectional area of the plate, cm^2
A_j	parameter characterizing magnitude of anodic reaction at the potential where the main reaction is beginning to reach limiting current (see equation 19)
A_{tot}	total superficial electrode area, cm^2
A_0	constant defined by equation 43
B	quantity defined in equation 54
c_i	concentration of species i per unit volume of solution, mol/cm^3
c_{io}	local surface concentration of species i, mol/cm^3
$c_{i,re}$	concentration of species i in the reference electrode compartment, mol/cm^3
$c_{i,ref}$	reference concentration of species i, mol/cm^3
$c_{i\infty}$	concentration of species i in the bulk, mol/cm^3
c_0	feed concentration to flow-through electrode, mol/cm^3
c_L	exit concentration of reactant, mol/cm^3
C	ratio of capital cost to fuel cost, A/cm^2
C_a	capital cost coefficient, $\$/cm^2$-s
C_d	electrical double-layer capacity, F/cm^2
C_e	electric energy cost, \$/J
C_f	fuel cost coefficient, \$/C
D'	dimensionless dispersion coefficient defined in equation 54
D_a	dispersion coefficient, cm^2/s
D_i	diffusion coefficient of species i, cm^2/s
D_{ij}	diffusion coefficient for interaction of species i with species j, cm^2/s
F	Faraday's constant, 96487 C/equiv
F_a	flow rate of inerts on anode side, mol/s
g	acceleration of gravity, cm/s^2

h	spacing between electrodes, cm
$\mathbf{i}$	current density, A/cm^2
i_j	current density for reaction j, A/cm^2
i_n	transfer current per unit of interfacial area, A/cm^2
i_0	exchange current density, A/cm^2
$\mathbf{i}_1$	superficial current density in the matrix, A/cm^2
$\mathbf{i}_2$	superficial current density in the pore phase, A/cm^2
$i_{m,lim}$	limiting current density for the main reaction, A/cm^2
$i_{oj,ref}$	exchange current density for reaction j with reference concentrations, A/cm^2
I	current density, A/cm^2, or total current leaving tab, A
j_{in}	pore-wall flux of species i, mol/cm^2
k_m	coefficient of mass transfer between flowing solution and electrode surface, cm/s
K_u	resale value of unused but depleted hydrogen, as a fraction of value in feed
L	length of planar electrodes, or length of porous electrode, cm
L_p	thickness of positive electrode, cm
L_{bus}	length of interconnecting bus, cm
L_{post}	length of interconnecting post, cm
M	current collector weight, g
M_i	molecular weight of species i, g/mol
n	number of electrons transferred in electrode reaction, equiv/mol
n_j	number of electrons transferred in reaction j, equiv/mol
$\mathbf{N}_i$	flux of species i, or superficial flux of species i, mol/cm^2-s
p	pressure, dyne/cm^2
p_{H_2}	partial pressure of hydrogen at the anode, bar
p_{O_2}	partial pressure of oxygen at the cathode, bar
P	electric power produced, W
R	universal gas constant, 8.3143 J/mol-K
R'	effective ohmic resistance, Ω-cm^2

R_g	resistance of grid, Ω-cm^2
R_i	rate of homogeneous production of species i, mol/cm^3-s, or sum of internal area specific resistances, Ω-cm^2
R_s	separator resistance, Ω-cm^2
$R_{a,1}$	anode matrix resistance, Ω-cm^2
$R_{a,2}$	anolyte solution resistance, Ω-cm^2
$R_{c,1}$	cathode matrix resistance, Ω-cm^2
$R_{c,2}$	catholyte solution resistance, Ω-cm^2
R_F	Faradaic charge-transfer resistance, Ω-cm^2
Re	Reynolds number
s_i	stoichiometric coefficient of species i in electrode reaction
s_{ij}	stoichiometric coefficient of species i in reaction j
Sc	Schmidt number
t	time, s
T	absolute temperature, K
u	fractional utilization of hydrogen
u_i	mobility of species i, cm^2-mol/J-s
U	apparent open-circuit potential, V
U'	constant in equation 22, V
$U_{j,o}$	theoretical open-circuit potential for reaction j at the composition prevailing locally at the electrode surface relative to a reference electrode of a given kind, V
$U_{j,ref}$	theoretical open-circuit potential evaluated with reference concentrations, V
U_j^θ	standard electrode potential of reaction j, V
U_{re}^θ	standard potential for the reference electrode reaction, V
ΔU_s	approximate length of the limiting current plateau for the main reaction before the onset of the side reaction, V
$\mathbf{v}$	solution velocity or superficial fluid velocity, cm/s
$\langle v \rangle$	average solution velocity, cm/s
V	electrode potential or cell potential, V

V_m	electrode potential where main reaction begins to reach limiting current, V
ΔV	voltage displacement from open circuit, V
x	distance through porous electrode, cm
X_{H_2}	ratio of moles of H_2 to moles of inerts
y	$=ak_m/v$, dimensionless distance
Y	electrochemical conductance, Ω^{-1}-cm^{-2}
Y_0	electrochemical conductance at start of discharge, Ω^{-1}-cm^{-2}
z_i	valence or charge number of species i

GREEK LETTERS

α	$= ak_m/v$, reciprocal reaction distance, cm^{-1}
α_a	transfer coefficient in anodic direction
α_{aj}	anodic transfer coefficient for reaction j
α_c	transfer coefficient in cathodic direction
α_{cj}	cathodic transfer coefficient for reaction j
γ_{ij}	exponent in composition dependence of exchange current density
δ	dimensionless current density defined in equation 61
ϵ	porosity or void volume fraction, dimensionless, or permittivity, F/cm
η_{cj}	concentration overpotential for reaction j, V
η_s	surface overpotential, V
η_{sj}	surface overpotential for reaction j, V
θ	$= c_i/c_0$, dimensionless concentration
θ_L	$= c_L/c_0$, dimensionless exit concentration
κ	effective conductivity of solution, Ω^{-1}-cm^{-1}
λ	Debye length, cm
μ	viscosity, g/cm-s

μ_i	electrochemical potential of species i, J/mol
ν	kinematic viscosity of the solution, cm^2/s
ν^2	dimensionless exchange current given by equation 62
Π_1	$= I/2AY\Delta V$, dimensionless plate current
Π_2	$= M\sigma/\rho YA^2$, ratio of grid to electrochemical conductance, dimensionless
Π_3	$= M/\rho L_p A$, volume fraction or grid, dimensionless
ρ	density, g/cm^3
ρ_o	pure solvent density, kg/cm^3
σ	effective conductivity of the matrix phase, or the conductivity of the current collecting grid, Ω^{-1}-cm^{-1}
Φ	electrostatic potential, V
$\tilde{\Phi}_o$	potential in the bulk solution extrapolated to the electrode surface, V
$\Delta\tilde{\Phi}_{ohm}$	ohmic potential drop in the absence of concentration variations, V
Φ_1	electric potential in the matrix, V
Φ_2	electric potential in the solution, V
Φ_p	potential of the positive plate, V
Φ_n	potential of the negative plate, V

SUBSCRIPTS

g	reference electrode of a given kind
i	species i
j	reaction j
m	main reaction
o	electrode surface, solvent, reactor inlet, or beginning of discharge
ohm	ohmic
$r1$	reference electrode located just outside the double layer
$r2$	reference electrode in the bulk solution

re	reference electrode
ref	reference concentrations
s	side reaction, or reference electrode of the same kind as the working electrode
∞	bulk solution
1	porous electrode matrix phase
2	porous electrode solution phase

SUPERSCRIPTS

exit	exit stream
o	feed stream

References

1. W. Bruce Darlington and Marino Y. C. Woo, "Report of the Electrolytic Industries 1981," Report sponsored by the Industrial Electrolytic Division of the Electrochemical Society, May 12, 1982.

2. C. L. Mantell, *Electrochemical Engineering*, 4th Edition, McGraw Hill, New York, 1960, p. 391.

3. *1980 Annual Survey of Manufactures*, M80(AS)-1, U.S. Department of Commerce, p. 14.

4. *Assessment of Research Needs for Advanced Battery Systems*, NMAB-390, National Materials Advisory Board, Commission on Engineering and Technical Systems, National Research Council, 1982, p. 183.

5. T. R. Beck, in *Proceedings of the Workshop on Energy Conservation in Industrial Electrochemical Processes*, Argonne National Laboratory Report No. ANL/OEPM-77-1, August 1976, 37-82.

6. J. O'M. Bockris, Brian E. Conway, Ernest Yeager, Ralph E. White, eds., *Comprehensive Treatise of Electrochemistry, Volume 2: Electrochemical Processing*, Plenum, New York (1981).

7. G. M. Wenglowski, "An Economic Study of the Electrochemical Industry in the United States," J. O'M. Bockris, ed., *Modern Aspects of Electrochemistry*, **4**, Butterworths, London, 1966, 251-306.

8. Jean Van Muylder, "Thermodynamics of Corrosion," J. O'M. Bockris, Brian E. Conway, Ernest Yeager, Ralph E. White, eds., *Comprehensive Treatise of Electrochemistry, Volume 4: Electrochemical Materials Science*, Plenum, New York (1981).

9. A. T. Kuhn, ed., *Industrial Electrochemical Processes*, Elsevier, New York (1971).

10. R. W. Houghton and A. T. Kuhn, "Mass-transport Problems and Some Design Concepts of Electrochemical Reactors," *Journal of Applied Electrochemistry*, **4** (1974), 173-190.

11. John Newman, "Engineering Design of Electrochemical Systems," *Industrial and Engineering*

Chemistry, **60**, No. 4 (April, 1968), 12-27.

12. John Newman, *Electrochemical Systems*, Prentice-Hall, Englewood Cliffs, New Jersey (1973).

13. David C. Grahame, "The Electrical Double Layer and the Theory of Electrocapillarity," *Chemical Reviews*, **41** (1947), 441-501.

14. Allen J. Bard and Larry R. Faulkner, *Electrochemical Methods, Fundamentals and Applications*, Wiley, New York, 1980.

15. Paul Delahay, *Double Layer and Electrode Kinetics*, Interscience Publishers, New York, 1965.

16. Roger Parsons, "Equilibrium Properties of Electrified Interfaces," *Modern Aspects of Electrochemistry*, **1** (1954), 103-179.

17. Ralph Edward White, *Simultaneous Reactions on a Rotating Disk Electrode*, dissertation, University of California, Berkeley (March, 1977).

18. J. L. Fitzjohn, "Electro-organic Synthesis," *Chemical Engineering Progress*, **71** (1975), 85-91.

19. George P. Sakellaropoulos, "Criteria for Selective Path Promotion in Electrochemical Reaction Sequences," *AIChE Journal*, **25** (1979), 781-793.

20. George P. Sakellaropoulos and Gary A. Francis, "Electrochemical Reactor Analysis: Selectivity of Multiple Competing Reactions," *Journal of the Electrochemical Society*, **126** (1979), 1928-1937.

21. George P. Sakellaropoulos and Gary A. Francis, "Selectivity and Reactor Analysis for Parallel Electrochemical Reactions," *Journal of Chemical Technology and Biotechnology*, **30** (1980), 102-109.

22. W. R. Parrish and John Newman, "Current Distribution on a Plane Electrode below the Limiting Current," *Journal of the Electrochemical Society*, **116** (1969), 169-172.

23. W. R. Parrish and John Newman, "Current Distributions on Plane, Parallel Electrodes in

Channel Flow," *Journal of the Electrochemical Society*, **117** (1970), 43-48.

24. Reinaldo Cabán and Thomas W. Chapman, "Rapid Computation of Current Distribution by Orthogonal Collocation," *Journal of the Electrochemical Society*, **123** (1976), 1036-1041.

25. Johnsee Lee and J. R. Selman, "Effects of Separator and Terminal on the Current Distribution in Parallel-Plate Electrochemical Flow Reactors," *Journal of the Electrochemical Society*, **129** (1982), 1670-1678.

26. Jacob Jorné, "Mass Transfer in Laminar Flow Channel with Porous Wall," *Journal of the Electrochemical Society*, **129** (1982), 1727-1733.

27. John Newman, "The Fundamental Principles of Current Distribution and Mass Transport in Electrochemical Cells," Allen J. Bard, ed., *Electroanalytical Chemistry*, **6**, Marcel Dekker, New York, 1973.

28. D. J. Pickett, *Electrochemical Reactor Design*, Second Edition, Elsevier, New York, 1979.

29. Ralph White and John Newman, "Simultaneous Reactions on a Rotating-Disk Electrode," *Journal of Electroanalytical Chemistry*, **82** (1977), 173-186.

30. John Newman, "Optimization of Potential and Hydrogen Utilization in an Acid Fuel Cell," *Electrochimica Acta*, **24** (1979), 223-229.

31. N. Ibl and E. Adam, "Optimierung in der Elektrochemischen Verfahrenstechnik," *Chemie Ingenieur Technik*, **37** (1965), 573-581.

32. N. Ibl and P. M. Robertson, "Optimisation of use of Surplus Night Electricity in Electrochemical Processes," *Electrochimica Acta*, **18** (1973), 897-906.

33. N. Ibl, "Optimization of Copper Refining," *Electrochimica Acta*, **22** (1977), 465-477.

34. Richard C. Alkire, Gary D. Cera, and Mark A. Stadtherr, "Optimization of Electrolytic Cells

Having Large Numbers of Variables," *Journal of the Electrochemical Society*, **129** (1982), 1225-1231.

35. John Newman and William Tiedemann, "Flow-through Porous Electrodes," *Advances in Electrochemistry and Electrochemical Engineering*, **11** (1978), 353-438.

36. John Newman and William Tiedemann, "Porous-Electrode Theory with Battery Applications," *AIChE Journal*, **21** (1975), 25-41.

37. Douglas N. Bennion and John Newman, "Electrochemical removal of copper ions from very dilute solutions," *Journal of Applied Electrochemistry*, **2** (1972), 113-122.

38. John Van Zee and John Newman, "Electrochemical Removal of Silver Ions from Photographic Fixing Solutions Using a Porous Flow-Through Electrode," *Journal of the Electrochemical Society*, **124** (1977), 706-708.

39. Michael Matlosz and John Newman, "Use of A Flow-Through Porous Electrode for Removal of Mercury from Contaminated Brine Solutions," *Proceedings of the Symposium on Transport Processes in Electrochemical Systems* (The Electrochemical Society, volume 82-10, 1982), 53-63.

40. M. Fleischmann, J. W. Oldfield and L. Tennakoon, "Fluidized bed electrodes Part IV. Electrodeposition of copper in a fluidized bed of copper-coated spheres," *Journal of Applied Electrochemistry*, **1** (1971), 103-112.

41. S. Germain and F. Goodridge, "Copper Deposition in a Fluidised Bed Cell," *Electrochimica Acta*, **21** (1976), 545-550.

42. Sherlock Swann, Jr. and Richard Alkire, *Bibliography of Electro-Organic Syntheses 1801-1975*, The Electrochemical Society, Incorporated, Princeton, NJ, 1980.

43. G. L. Wierschem and W. H. Tiedemann, "Cycling Behavior of Lead-Acid Batteries for Electric Vehicles," Abstract Number 102, Hollywood, Florida meeting of the Electrochemical Society,

October 1980.

44. Liebenow, "Über die Berechnung der Kapazität eines Bleiakkumulators bei variabeler Stromstärke," *Zeitschrift für Elektrochemie*, **4** (1897), 58 (particularly p. 63).

45. Peter W. Appel and John Newman, "Application of the Limiting Current Method to Mass Transfer in Packed Beds at Very Low Reynolds Numbers," *AIChE Journal*, **22** (1976) 979-984.

46. Peter S. Fedkiw and John Newman, "Mass-Transfer Coefficients in Packed Beds at Very Low Reynolds Numbers," *International Journal of Heat and Mass Transfer*, **25** (1982), 935-943.

47. William G. Gray, "A Derivation of the Equations For Multi-Phase Transport," *Chemical Engineering Science*, **30** (1975), 229-233.

48. John Stephen Dunning, *Analysis of Porous Electrodes with Sparingly Soluble Reactants*, dissertation, University of California, Los Angeles (1971).

49. Peter Fedkiw and John Newman, "Low Péclet Number Behavior of the Transfer Rate in Packed Beds," *Chemical Engineering Science*, **33** (1978), 1043-1048.

50. Richard Pollard and John Newman, "Transport Equations for a Mixture of Two Binary Molten Salts in a Porous Electrode," *Journal of the Electrochemical Society*, **126** (1979), 1713-1717.

51. P. V. Danckwerts, "Continuous flow systems. Distribution of Residence Times," *Chemical Engineering Science*, **2** (1953), 1-13.

52. J. F. Wehner and R. H. Wilhelm, "Boundary conditions of flow reactor," *Chemical Engineering Science*, **6** (1956), 89-93.

53. James A. Trainham and John Newman, "The Effect of Electrode Placement and Finite Matrix Conductivity on the Performance of Flow-Through Porous Electrodes," *Journal of the Electrochemical Society*, **125** (1978), 58-68.

54. Richard Alkire and Patrick K. Ng, "Two-Dimensional Current Distribution Within a Packed-Bed Electrochemical Flow Reactor," *Journal of the Electrochemical Society,* **121** (1974), 95-103.

55. James A. Trainham and John Newman, "A Comparison between Flow-Through and Flow-By Porous Electrodes for Redox Energy Storage," *Electrochimica Acta,* **26** (1981), 455-469.

56. Peter S. Fedkiw, "Ohmic Potential Drop in Flow-Through and Flow-By Porous Electrodes," *Journal of the Electrochemical Society,* **128** (1981), 831-838.

57. William Tiedemann, *Electrochemical Engineering of Batteries,* Short Course Lecture Notes, University of California, Los Angeles, California, May 1978.

58. John S. Dunning, Douglas N. Bennion, and John Newman, "Analysis of Porous Electrodes with Sparingly Soluble Reactants," *Journal of the Electrochemical Society,* **118** (1971), 1251-1256.

59. King Wai Choi, Douglas N. Bennion, and John Newman, "Engineering Analysis of Shape Change in Zinc Secondary Electrodes I. Theoretical," *Journal of the Electrochemical Society,* **123** (1976), 1616-1627.

60. King Wai Choi, Drannan Hamby, Douglas N. Bennion, and John Newman, "Engineering Analysis of Shape Change in Zinc Secondary Electrodes II. Experimental," *Journal of the Electrochemical Society,* **123** (1976), 1628-1637.

61. S.B. Brummer, K.M. Abraham, V.R. Koch, and G.L. Holleck, *Review of the Status of Ambient-Temperature Secondary Lithium Batteries for Applicability to Load Levelling and Electric Vehicles,* EIC Corporation, Newton, Massachusetts, July 1980.

62. John S. Newman and Charles W. Tobias, "Theoretical Analysis of Current Distribution in Porous Electrodes," *Journal of the Electrochemical Society,* **109** (1962), 1183-1191.

63. Richard Pollard and John Newman, "Mathematical Modeling of the Lithium-Aluminum, Iron Sulfide Battery I. Galvanostatic Discharge Behavior," *Journal of the Electrochemical Society,* **128**

(1981), 491-502.

64. D.L. Barney and others, *Lithium/Iron Sulfide Batteries for Electric-Vehicle Propulsion and Other Applications*, Progress Report for October 1979-September 1980, p. 71, Argonne, Illinois, Argonne National Laboratory, February 1981. (ANL-80-128)

65. W. H. Tiedemann and J. Newman, "Nonuniform Current and Potential Distribution in Composite Sheet Type Battery Electrodes," Abstract number 169, Los Angeles, California meeting of the Electrochemical Society, October 1979.

66. William H. Tiedemann and John Newman, "Current and Potential Distribution in Lead-Acid Battery Plates," *Proceedings of the Symposium on Battery Design and Optimization* (The Electrochemical Society, volume 79-1, 1979), 39-49.

67. William H. Tiedemann and John Newman, "Mathematical Modeling of the Lead-Acid Cell," *Proceedings of the Symposium on Battery Design and Optimization* (The Electrochemical Society, volume 79-1, 1979), 23-38.

This report was done with support from the Department of Energy. Any conclusions or opinions expressed in this report represent solely those of the author(s) and not necessarily those of The Regents of the University of California, the Lawrence Berkeley Laboratory or the Department of Energy.

Reference to a company or product name does not imply approval or recommendation of the product by the University of California or the U.S. Department of Energy to the exclusion of others that may be suitable.

TECHNICAL INFORMATION DEPARTMENT
LAWRENCE BERKELEY LABORATORY
UNIVERSITY OF CALIFORNIA
BERKELEY, CALIFORNIA 94720